1	Molecular level Insights on the Photosensitized Chemistry of Nonanoic Acid in	
2	the Presence of 4-Benzoylbenzoic Acid at the Sea Surface Microlayer Surface-	
3	Bulk Photochemical Coupling of Nonanoic Acid and 4-Benzoylbenzoic Acid:	
4	The Dual Role of the Photosensitizer and Environmental Influences	
5		
6	Ahmed Abdelmonem ^{1,*} , Dana Glikman ² , Yiwei Gong ¹ , Björn Braunschweig ² , Harald	
7	Saathoff ¹ , Johannes Lützenkirchen ³ , and Mohammed H. Fawey ⁴	
8		
9 10	1. Institute of Meteorology and Climate Research, Karlsruhe Institute of Technology (KIT), 76344 Eggenstein- Leopoldshafen, Germany	
11	2. Institute of Physical Chemistry and Center for Soft Nanoscience, University of Münster, 48149 Münster, Germany	
12 13	3. Institute of Nuclear Wastes Disposal, Karlsruhe Institute of Technology (KIT), 76344 Eggenstein-Leopoldshafen, Germany	
14	4. Physics Department, Faculty of Science, Sohag University, 82524 Sohag, Egypt.	
15	* Corresponding Author: ahmed.abdelmonem@kit.edu	

1 Abstract

2 Atmospheric chemistry and aerosol-water interactions significantly impact Earth's climate by influencing the energy budget. Organic compounds concentrated at air-water interfaces, 3 such as the sea—surface microlayer (SML), or aerosol and cloud droplets, are key contributors to 4 5 atmospheric aerosols and undergo complex photochemical reactions. Nonanoic acid (NA) is surface active and 4-benzoylbenzoic acid (4-BBA) is a photosensitizer. This study combines investigations 6 7 at the air water interface by sum-frequency generation (SFG) spectroscopy and in the liquid and gas 8 phases by mass spectrometry (MS) to investigate study the photochemical interactions of nonanoic acid (NA) and 4 benzoylbenzoic acid (4 BBA)both substances at the air-water interface. 9 We identify a novel interfacial aromatic signal via SFG, revealing surface-localized photoproducts 10 previously undetected (C₉H₁₀O₅).under varying solar spectra, pH, and salinity conditions. SFG 11 spectroscopy detected aromatic signals at the interface, unreported in prior studies using bulk 12 techniques, highlighting the partitioning of non-surface-active compounds to the organic surface 13 layer. The study demonstrates that 4-BBA not only acts both as a photosensitizer but also undergoes 14 photodegradationand a photoproduct precursor, with its photolysis being more active under shorter 15 UV wavelengths. Our experiments show the critical influence of the UV portion of the solar spectrum 16 on photoproduct formation, as significant amounts of benzene (C₆H₆) and benzaldehyde (C₇H₆O) 17 18 were detected as degradation products of 4-BBA in the gas phase particularly for the lowest 19 wavelengths (280-310 nm). In the liquid phase, we identified the following photoreaction products: $C_8H_{12}O_4$, $C_8H_{12}O_5$, $C_9H_{10}O_5$, $C_9H_{14}O_3$, $C_9H_{16}O_3$, $C_9H_{16}O_4$, and $C_{10}H_{14}O_4$. Among these, $C_8H_{12}O_4$, 20 C₉H₁₀O₅, and C₉H₁₆O₃ were most enhanced (by a factor of ~11) in the presence of 4-BBA, with 21 22 C₉H₁₀O₅ strongly dependent on the presence of oxygen. The formation of C₉H₁₀O₅ increased at shorter wavelengths due to photodegradation of 4-BBA, while C₈H₁₂O₄ and C₉H₁₆O₃ were dominant 23 24 at longer wavelengths, consistent with photooxidation of NA. Reactio While pH and salinity were not varied systematically in this study, we found that decreasing the pH from 8 to 5.4 affected the water 25 restructuring at the interface and increased the rate of photoproducts formation. Increasing salinity 26 27 from zero to ~ 38 ppt enhanced the photoreaction rates by a factor of two. These findings highlight the importance of environmental factors in modeling interfacial photochemistry and demonstrate how 28 SFG reveals surface—bulk coupling relevant to aerosol formation in diverse aquatic systems.n 29 mechanisms were found to depend on solar spectrum, pH, and salinity, with salinity accelerating 30 photoreaction rates by increasing surface concentrations of 4-BBA. These findings emphasize the 31 32 need to account for environmental variables such as light intensity, geographic location, and 33 atmospheric conditions when modeling photochemical processes. The results provide insights into

1	surface bulk photochemical coupling and their implications for aerosol formation across diverse
2	natural water systems, from oceans to cloud droplets.
3	
4	
5	<u>Keywords</u> : Sum-frequency generation (SFG) spectroscopy; Mass spectrometry; <u>Air-water Air-water</u>
6	interface; Sea surface microlayer; Aerosol formation; volatile Volatile organic
7	compounds.

1. Introduction

1

2 The Earth's climate system is impacted by atmospheric chemistry and aerosol-waterair-water interactions, which affect the energy budget through scattering of sunlight and absorption of thermal 3 radiation (Meerkötter and Vázquez-Navarro, 2012). Atmospheric aerosols have both natural and 4 5 anthropogenic human made sources which vary depending on the location, time of year, and meteorological conditions (Boucher, 2015). These Sources include natural sources (e.g. dust, sea 6 7 spray, volcanic ash, wildfires, and biological particles), anthropogenic sources (e.g., industrial and 8 agricultural processes, transportation, and energy production), secondary formation (e.g. through 9 chemical reactions between pollutants in the atmosphere), and waste disposal (e.g. landfills, open burning) (Ouafo-Leumbe et al., 2018). It has been estimated that the secondary reaction products of 10 volatile organic compounds (VOCs) can make up acontribute significantly fraction ofto secondary 11 atmospheric aerosols (SOA), influencing cloud properties and radiative balance, with the vast 12 majority originating from biogenic sourcesparticularly in urban and industrial areas (Wang et al., 13 2023). It has been shown that Moreover, up to 91.9 TgC per year of organic vapors could be emitted 14 from the oceans into the marine atmosphere and have a potential contribution to organic aerosol mass 15 of more than 60 % over the remote ocean (Brüggemann et al., 2018). 16 17 Organic compounds are highly concentrated at the sea-surface microlayer (SML) or as surfactant coatings on cloud droplets (Carpenter and Nightingale, 2015). The SML contains dissolved organic 18 19 carbon (DOC) and chromophoric and fluorescent dissolved organic matter (CDOM and FDOM, respectively), which are transferred to the atmosphere via sea spray aerosol (SSA) (Yang et al., 2022) 20 21 . While sea salt dominates the cloud condensation nuclei (CCN) activity of SSA, organic matter 22 contributes primarily to aerosol mass (Hendrickson et al., 2021)-. Biological and physicochemical 23 processes in the SML, such as the enrichment of long- and medium-chain fatty acids (LCFAs and MCFAs), further enhance SSA surface activity and influence atmospheric processes (Dommer et al., 24 2024)-. Atmospheric nutrient deposition can also influence short-term enrichments of organic matter 25 in the SML, particularly when associated with biomass burning emissions (Milinković et al., 2022). 26 27 The air-water interface is ubiquitous in the environment and frequently exposed to the 28 atmosphere and/or solar light, making photochemical interactions highly probable (Liss and Duce, 29 2005), particularly in the presence of light-absorbing Ceompounds, such as chromophoric dissolved organic matter DOM, which is more concentrated at surfaces. It was previously believed that CDOM 30 31 is more concentrated at surfaces than in the bulk than in bulk (Carlson, 1983; Carlson and Mayer, 1980), however, more recent studies have shown that CDOM is not always enriched at the surface 32 (van Pinxteren et al., 2020; Stolle et al., 2020; Tilstone et al., 2010). -Organic coatings on water 33 surfaces are a significant source of atmospheric aerosols, either through direct emission to the 34

atmosphere, such as sea spray, or indirect emission through the generation of new products from 1 2 photo interactions on the surface exposed to solar radiation. The presence of organic coatings on water surfaces can increase the concentration of natural photosensitizers and facilitate the generation 3 of reactive species and VOCs through photochemical and oxidative processes, leading to an increased 4 5 rate of photochemical reactions (Tinel et al., 2016; Wang et al., 2023)(Tinel et al., 2016),...Ozone 6 oxidation in the SML, for example, generates VOCs such as acetone and aldehydes (Wang et al., 2023). Photobleaching of CDOM leads to the formation of low-molecular-weight DOM and CO₂, 7 with reaction rates dependent on solar radiation intensity and DOM composition (Yang et al., 2022) 8 9 . This process is influenced by the intensity and duration of solar radiation, as well as the composition 10 of DOM, which varies seasonally and spatially. 11 Solar radiation and wind intensity shape SML chemistry by modifying organic content and regulating air-sea CO2 exchange (Stolle et al., 2020). -Natural bodies of water, including lakes, rivers, and 12 oceans, exhibit a range of varying pH and salinity values and mineral contents, which are influenced 13 by a range of atmospheric, geological, and biological processes. Ttypically, the pH of natural water 14 15 bodies varies between pH 6 and 9 (Dickson, 1993; Jiang et al., 2019) and the salinity can range between 0.5 ppt, for fresh water, (parts per thousand) (Dommer et al., 2024) and 35 ppt, for ocean 16 (Millero et al., 2008), although. However, certain factors, such as hydrogeochemical acid rain or 17 18 specific geological formations factors, can cause the pH and salinity to cross these limits deviations (Cui et al., 2022). Moreover, tThe presence of minerals ions such as calcium, magnesium, sodium, 19 chloride, and sulfate can further influence the salinity and also pH, thereby modulating the surface 20 activity of the organic compounds (Covington and Whitfield, 1988; Marion et al., 2011), which thus 21 22 contributes in two ways to the surface activity of the organic compounds. These mineral content and 23 pH of the natural bodies of watergeochemical parameters play a vital roles in their chemical and 24 physical processes such as rock weathering, mineral precipitation, gas solubility, corrosion, biological 25 shell formation, and water hardness (Morgan, 1995). 26 Prior reports on the existence and significance of organic layers at air-water interfaces, such 27 as the SML (Bernard et al., 2016; Ciuraru et al., 2015; Mmereki and Donaldson, 2002; Tinel et al., 2016) and sea spray (Sellegri et al., 2006; Wilson et al., 2015), emphasized the need to investigate 28 29 this critical interface, particularly at the molecular level and under atmospheric conditions. Recent 30 studies have highlighted the critical role of ocean biogeochemistry in shaping atmospheric composition and influencing aerosol-cloud interactions. In particular, the sea surface microlayer has 31 32 been recognized as a key interface for biologically driven gas emissions, with important implications 33 for their representation in large-scale atmospheric models (Tinel et al., 2023)—. Moreover, oceanic 34 biogeochemical processes have been shown to affect aerosol formation and cloud properties, thereby

contributing to climate-relevant feedback mechanisms (Sellegri et al., 2024)-. Despite numerous 1 2 studies aimed at investigating the emission and uptake of gases and aerosols (e.g. VOCs, secondary organic aerosol (SOA) particles, and trace gases) in the atmosphere, limited information is available 3 on the molecular composition and structure of surface entities (e.g. adsorbed on cloud droplets or sea 4 5 surfaces) and their role in influencing interactions. A deeper understanding is urgently needed, as 6 interfacial chemistry strongly governs atmospheric reactivity. There is a continued urgency to 7 comprehend fundamental processes at this interface, as it is widely known that atmospheric reactions 8 are highly dependent on the interfacial layers. 9 The air-waterair-water surface interactions occur in a variety of bodies of water and involve both biogenic and abiotic emissions (Bernard et al., 2016; Brüggemann et al., 2018), with organic materials 10 from the SML being emitted into the atmosphere through bubble bursting and forming sea-spray 11 aerosols (Gantt and Meskhidze, 2013; Sellegri et al., 2006). These organic materials can be oxidized 12 in the air and contribute to the creation of SOAs, which can then act as ice nuclei in mixed-phase 13 14 clouds and high-altitude ice clouds (Liss and Duce, 2005). In recent years, the study of the air water 15 interface has received increasing attention in atmospheric research (Alpert et al., 2017; Bernard et al., 16 2016; Carpenter and Nightingale, 2015; Ciuraru et al., 2015; Gantt and Meskhidze, 2013; Liss and Duce, 2005; Sellegri et al., 2006; Tinel et al., 2016; Wilson et al., 2015). Tinel et al. (2016) (Tinel et 17 18 al., 2016) demonstrated that the photosensitized degradation of fatty acids at the air—water interface, specifically nonanoic acid (NA) in the presence of 4-benzoylbenzoic acid (4-BBA) and imidazole-2-19 20 carboxaldehyde as model systems, enhances VOC emissions and secondary aerosol formation Tinel et al. (2016) revealed that the photosensitized chemistry of fatty acids at the air-water interface leads 21 22 to unique interactions under atmospheric conditions (Tinel et al., 2016). The authors examined the 23 photodegradation of Nonanoic acid (NA), a simple fatty acid, in the presence of two natural 24 photosensitizers, 4-benzoylbenzoic acid (4-BBA) and imidazole-2-carboxaldehyde. The study showed that organic coatings on the water surface can enhance the concentration of natural 25 photosensitizers at the air-water interface, promoting specific photochemical reactions that impact 26 the composition and concentration of VOCs (Tinel et al., 2016) emitted into the atmosphere. A 27 subsequent study by Alpert et al. (2017) reported the formation of SOA particles through 28 photochemical reactions and ozonolysis of saturated long-chain fatty acids and alcohol surfactants at 29 the water surface Additionally, the authors reported the production of SOA particles following 30 photochemical reactions and ozonolysis of saturated long-chain fatty acids and alcohol surfactants at 31 the water surface (Alpert et al., 2017). (Alpert et al., 2017). More recently, Freeman-Gallant et al. 32 (2024) showed that the efficiency of NA photooxidation in thin films depends on the type of organic 33

1 photosensitizer, with 4-BBA identified as the most effective among those tested (Freeman-Gallant et

2 <u>al., 2024).</u>

6

7

8

9

10

11

12

13

14

15

16

17

18

19

20

21 22

23

24

25

26

27

28

29

30

31

32

Previous The prior experimental studies <u>primarily employed have largely utilized</u> chemical, elemental
 and linear spectroscopic methods (such as UV-visible absorption, laser-induced fluorescence, and

5 mass spectrometry). <u>In contrast, Mm</u>olecular-level spectroscopic data on air water interactions

insights into interfacial chemistry under atmospheric conditions are scarce., with limited in In-situ

information on molecular alignment, water-bonding, and the formation or degradation of chemical

surface functional groups remains limited, at the air-water interface. A molecular-level understanding

of gas-liquid interactions under atmospheric conditions and the factors that influence the reaction

mechanisms is but is critical to predicting the formation and degradation of for predicting aerosols

evolutions, and is therefore of fundamental importance.

In this work, we combine sum-frequency generation (SFG) spectroscopy and mass spectrometry (MS) to probe the interfacial and bulk-phase photoproducts, respectively, of a fatty acid being irradiated with different solar spectra at different pH and salinity at the air water interface. We studied the photochemical interactions of nonanoic acid (NA) at the water surface in the presence of 4benzoylbenzoic acid (4-BBA under varying irradiation spectra. We didn't vary pH, and salinity systematically but only report their impact for relatively small ranges). This system was particularly chosen due to the availability of prior bulk-phase study relying on linear techniques a reference work where only linear techniques were used to probe the photoproducts in the bulk phases (Tinel et al., 2016), which. The reference work verified that the interaction takes place at the water surface. Since SFG technique is suitable to probe the surface layer, we applied it here to probe the chemical and structural changes in the system. We detected an aromatic signal by the SFG upon the photoreaction which was not reported by the linear techniques used in the reference work. The changes in the SFG spectra with irradiation depend on the pH of the solution. We employed an LED solar simulator with a spectrum closely resembling natural sunlight, improving upon earlier Xenon lamp-based studies For the irradiation of the samples we use an LED solar simulator that produces a light spectrum that is closer to the solar spectrum than that of commercially available Xenon lamp that has been used in the reference work. The following section describes our experimental approach, followed by results and discussion beginning with the air-water interface and progressing to the molecular analysis of products in the aqueous and gas phases. We also studied the effect of pH, starting from a pH similar to the ocean to the normal pH. We found that the solar spectrum, pH and salinity affect the photoreaction rate by interfering mechanisms.

2. Experimental procedures

2.1 Materials

4-benzoylbenzoic acid (4-BBA, 95 %,) and nonanoic acid (NA, 97 %) were purchased from Sigma Aldrich and Alfa Aesar, respectively. NA was used as received without further purification. We did not observe any evidence that impurities in NA influenced the photochemical reactions under the irradiation conditions used in this study. In contrast, 4-BBA was purified due to the presence of surface-active impurities. All solutions were prepared using ultrapure water (18.2 M Ω -.cm; total oxidizable carbon <5 ppb) that was obtained from a Milli-Q Reference A+ (Merck) purification system). Unless stated otherwisementioned differently, all mixtures examined here are aqueous solutions of 2 mM NA and 0.2 mM 4-BBA and with a total volume of four milliliters. The solution of 4-BBA was prepared using ultrasonication for three hours and then steering over night at pH 7. The solution of NA was prepared using ultrasonication for one hour. The pH was adjusted using 0.1 M NaOH from Fischer Chemical and controlled with SevenExcellence pH/Cond meter S470 from METTLER TOLEDO. Lab experiments were conducted under either synthetic air (ALPHAGASTM, $20.5 \pm 0.5 \%$ O₂ in N₂) or Nitrogen gas (99.9999 %) from Air Liquid. The exact conditions for each experiment can be found in the supporting information (SI).

2.2 Db -4 - -b ---- -1

2.2 Photochemical reactor Light source

To study photochemistry under atmospheric conditions, an irradiation source that closely mimics solar light is essential. It should be tunable to simulate different latitudes, altitudes, and seasonal variations, requiring a wavelength range starting at ~275 nm, adjustable intensity, and homogeneous illumination. For this purpose, a compact custom-built LED-based solar simulator, the "Atmospheric Surface-Science Solar Simulator", was developed. The device is optimized to irradiate a 30 mm diameter sample area from a 50 mm distance, ensuring controlled photochemical reactions. The spectral characteristics of the simulator, including its spectral overlap with solar radiation and intensity adjustments, were determined using a calibrated spectrophotometer and a custom-built variable current source. In this work, two different irradiation spectra were employed to simulate solar radiation: AM1, representing ground-level sunlight after atmospheric filtering, and AM0, representing sunlight before absorption by the atmosphere, including wavelengths below 300 nm. Additionally, individual wavelengths (280, 310, 345, 365, 385, 405, 430, 470, 490, and 520 nm) as well as the UV portion of the AM0 spectrum were employed. Additional technical details, including LED spatial distribution, irradiation spectra of AM0 and AM1, and homogeneity calibration, are provided in the SI. The irradiation cell was placed on a large metal table that served as an effective

- 1 heat sink, inside a well temperature-controlled room. Quartz window allowed light to pass through
- 2 for irradiation. The LED light source emitted at wavelengths below 550 nm and produced no thermal
- 3 radiation. Cooling air from the light source electronics was vented away from the measurement cell.
- 4 Additional technical details, including LED spatial distribution, spectral comparisons, and
- 5 homogeneity calibration, are provided in the Supporting Information (SI).

7

2.3 SFG spectroscopy

- 8 Surface sum-frequency generation (SFG) spectroscopy is based on second-order nonlinear optical
- 9 effect that in dipole approximation only occurs where the inversion symmetry is broken which is
- always the case at interfaces between two phases (Miranda and Shen, 1999; Zhang et al., 1994). SFG
- is generated by a temporal and spatial overlap of two different frequency light pulses (usually visible
- and a tunable IR) at an interface between two isotropic media. It provides information about the
- interface by probing the individual species from their IR vibrational absorption (Shen, 1989). SFG
- has proven effective in probing aqueous solutions containing soluble ionic and molecular species,
- and in determining the role of these substances in changing the water structure at the interface (Schultz
- et al., 2002; Shultz et al., 2000). Surfactants partition to the interface and can displace or bind water
- into hydrated complexes. Various SFG investigations on air-water interfaces have centred
- on examining organic surfactants adsorbed at the water surface (Backus et al., 2012; Doughty et al.,
- 19 2016; Ghosh et al., 2009; Henry et al., 2003; Rao et al., 2011; Truong et al., 2019; Varga et al., 2005).
- 20 However, it is mandatory to focus on studies that include atmospherically relevant substances under
- 21 atmospheric conditions.
- The description of the SFG spectrometer used in this study can be found elsewhere (García Rey et
- al., 2019). The irradiation and ray geometry used in the present work are shown in Fig. S3SI. Details
- of the SFG experiments and data analysis can be found in the **Supporting Information SI** (Sect. S3).
- 25 The individual bands fitted to the different species are shown in Fig. S7. Table S2 lists the
- 26 experimental conditions of all SFG experiments conducted in this work. At first glance, due to the
- 27 distinguished feature of SFG as a sub-monolayer surface-sensitive technique, we realized that the
- delivered 4-BBA contained surface-active contaminants. The purple spectrum in Fig. S6 shows
- 29 vibrational bands in the CH region detected at the surface of a 0.2 mM aqueous solution of 4-BBA.
- 30 These bands are attributed to surface active organic contaminants in the solution. 4-BBA is not
- surface active (Mora Garcia et al., 2021) and there are no free CH bonds that could produce the CH-
- vibrations. To purify the 4-BBA, it was recrystallized twice from Ethanol. The green curve in Fig. S6
- shows the SFG spectrum of 4-BBA aquatic solution after the recrystallization. It is worth mentioning
- that we tested samples from different providers, including the provider mentioned in the reference

- work (Tinel et al., 2016), and found that 4-BBA was never delivered pure enough to not show surface-
- 2 active contaminants. The contamination in the 4-BBA should be considered when comparing our
- 3 results with those in the reference work.

5

2.4 Mass spectrometry

The analysis of liquid-phase products was carried out using the Filter Inlet for Gas and Aerosols 6 7 (FIGAERO, Aerodyne Inc.) in combination with a high-resolution time-of-flight chemical ionization 8 mass spectrometer (HR-ToF-CIMS, Aerodyne Inc.), employing I⁻⁻ as the ionization reagent. A 2.5 9 μL liquid sample was applied to a PTFE filter via a syringe and subsequently subjected to thermal desorption in FIGAERO-CIMS. To ensure that the sampled liquid solution was representative of the 10 entire system, the solution was thoroughly stirred prior to sampling to homogenize any surface-11 enriched compounds with the bulk. The syringe tip was then inserted into the center of the bulk phase 12 13 to draw the sample. Ultra-high-purity nitrogen served as the carrier gas, facilitating desorption as the temperature was gradually increased from 296 K to a peak of 473 K over 35 minutes. The total liquid-14 phase signal for each compound was determined by integrating its thermal desorption profile 15 (thermogram). Data processing was performed using Tofware software v3.1.2, with mass-to-charge 16 ratios adjusted by subtracting the reagent ion I... To enable comparisons, all ion signals were 17 normalized to 10⁶ cps I⁻⁻. Proton-transfer-reaction time-of-flight mass spectrometer (PTR-ToF-MS 18 4000, Ionicon Analytic GmbH) was utilized to measure the concentrations of gas-phase compounds. 19 20 The data was analyzed by PTR viewer 3.3.12. The gas phase was sampled by a syringe and transferred to the PTR-MS. Table S3 lists the experimental conditions of all MS experiments conducted in this 21 22 work. Since the photoreactor cannot be considered completely air-tight the measured concentrations cannot be converted into absolute yields of the gas phase reaction products. Results of the mass 23 24 spectrometry given in the results section were subtracted by the background signals measured in the 25 reference experiment MS_BG1. 26 The choice of analytical instrumentation significantly impacts the range and type of compounds 27 detected in complex samples. In the reference work by Tinel et al. (2016) (Tinel et al., 2016), after PFBHA derivatization, the use of reversed-phase ultra-performance liquid chromatography coupled 28 to high-resolution mass spectrometry (UPLC/(±)HESI-HRMS) allowed for the separation and 29 detection of a broad range of compounds from the aqueous phase. The FIGAERO-CIMS employed 30 in this study is particularly well-suited for the detection of semi- to low-volatile organic compounds, 31 32 especially for organic compounds with three or more oxygen atoms (Riva et al., 2019). Thus, the two techniques offer complementary insights, with UPLC-HRMS capturing a wider polarity range of 33 dissolved species and FIGAERO-CIMS covering products with higher O/C ratios. 34

1 3 Results and Discussion

2

32

33

3.1 SFG at the air-liquid interface

Figure 1 shows the SFG spectra at vaporair-water interface for NA, (a), and 4-BBA, (b), in dark 3 4 conditions and after exposure to AMO light (solar radiation spectrum before absorption by the atmosphere). AM0 was chosen because it includes the maximum portion of sun UV that can lead to 5 6 photo-induced chemistry in the atmosphere. Solution's pH was first adjusted to pH 8, which is the approximate pH value of the ocean (Jiang et al., 2019). Appropriate data fitting of the SFG spectrum 7 of NA in dark, black curve Fig. 1a, shows vibrational broad OH bands from hydrogen-bonded 8 interfacial water centered at ~3450 cm⁻¹ and ~3250 cm⁻¹, and narrow CH bands (CH₃ Fermi peak at 9 2946 cm⁻¹, CH₂ Fermi peak at 2917 cm⁻¹, CH₃ symmetric-stretch 2885 cm⁻¹, and CH₂ symmetric-10 stretch at 2858 cm⁻¹) (Lu et al., 2005; MacPhail et al., 1984; Snyder et al., 1982). The CH₂ Fermi 11 resonance appears as a shoulder next to the CH₃ Fermi peak and could be identified by the SFG data 12 fitting as shown in the SI. The so-called dangling OH band (~3700 cm⁻¹), which characterizes neat 13 air-water interfaces and arises from water molecules with one non-hydrogen-bonded OH group 14 pointing into the vapor phase (Sovago et al., 2008), was not detected in Fig. 1a. This indicates full 15 16 coverage of the water surface by NA. The dark SFG spectrum of 4-BBA, blue curve Fig. 1b, shows an SFG spectrum very similar to that of the neat air-water interface, black curve Fig. 1b. There are 17 no noticeable signs of 4-BBA at the interface, as expected, since 4-BBA is not surface-active. 18 As shown in the SFG spectra in Fig. 1a, AM0 irradiation of the 19 NA solution without 4-BBA produced no detectable changes in the SFG signal, indicating negligible 20 photoreactivity in the absence of 4-BBA. In contrast, Fig. 1b shows that while the OH stretching 21 modes of hydrogen-bonded interfacial water (~3250 and ~3450 cm⁻¹) remain within the signal-to-22 noise range upon AM0 irradiation of 4-BBA alone, a decrease in the dangling OH band (~3700 cm⁻¹ 23 1) is observed after 30 minutes of exposure (green curve) compared to the dark signal (blue curve). 24 Interestingly, after one hour of irradiation, the dangling OH signal (red curve) returns to its initial 25 intensity, matching the dark signal. Although subtle, these variations in the SFG signal suggest 26 perturbations in interfacial water structure, possibly due to the formation of photoproducts.no 27 considerable changes were observed upon exposure to AMO light, particularly for NA. The changes 28 in SFG spectra of air-water interfaces using 4-BBA solutions were within the signal-to-noise upon 29 different exposure to AMO irradiation. Although this is indicative for a neglectable influence of AMO 30 31 irradiation on pure 4-BBA solutions, a small drop in the SFG signals from the air-water interface after

30 min of irradiation time and a subsequent increase in the signal can be seen.

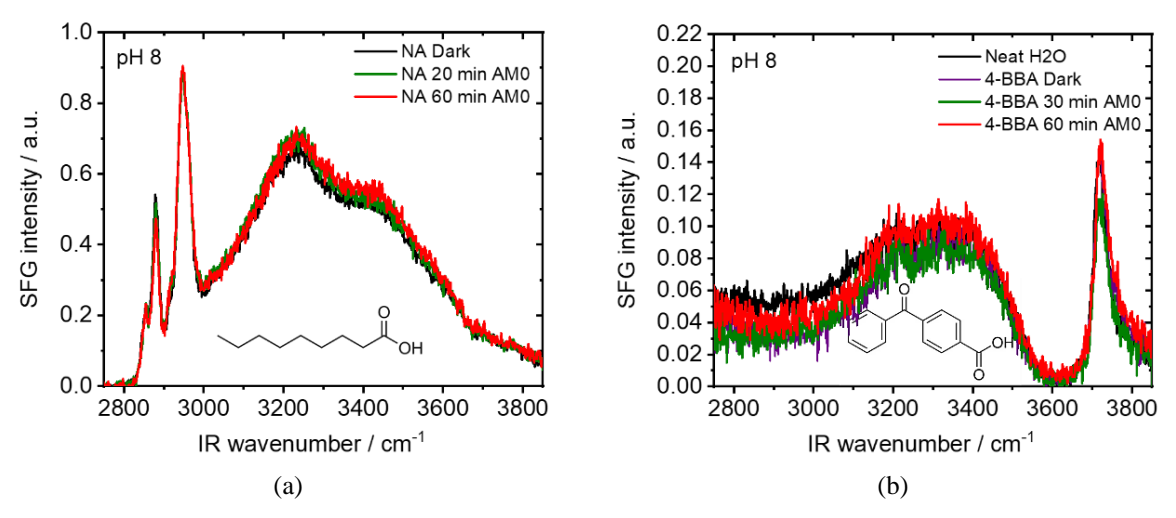


Figure 1: SFG at (a) <u>air-waterair-water</u> interface for NA (2mM), and (b) 4-BBA (0.2mM) as a function of time in dark conditions and after exposure to AM0 light. Both solutions were adjusted to pH 8.

2

3

4

5

6

7

8

9

10

11

12

13

14

15

16

17

18

19

20

21

22

23

24

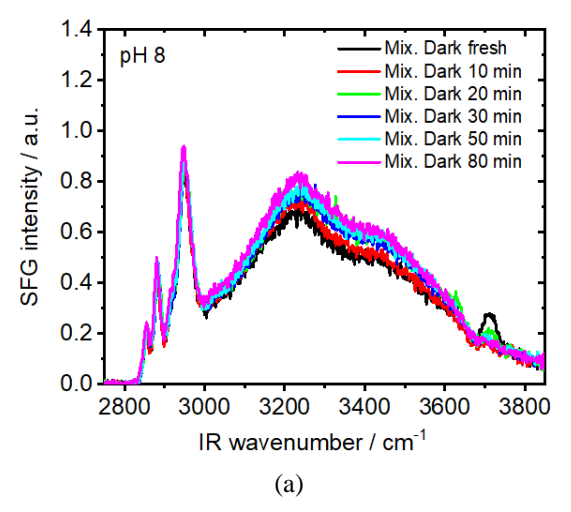
25

26

Figure 2a shows the SFG spectra from air-water interfaces for mixtures of NA and 4-BBA at a solution pH 8 as a function of time after which the interface was established, while the samples were continuously kept in the dark conditions (no light exposure). There is a visible change in the signal along the whole frequency range. At the beginning of the experiment, the SFG spectrum of the mixture shows a vibrational band that is attributable to the so-called dangling OH (~3700 cm⁻¹) mode from water molecules at the interface that have one non-hydrogen bonded OH group pointing into the vapor phase (Sovago et al., 2008). Additional broad OH bands from interfacial water are centered at ~3450 cm⁻¹ and ~3240 cm⁻¹, while CH vibrational bands (CH₃-Fermi peak at 2946 cm⁻¹, CH₂-Fermi peak at 2917 cm⁻¹, CH₃ symmetric-stretch 2885 cm⁻¹, and CH₂ symmetric-stretch at 2858 cm⁻¹) (Lu et al., 2005; MacPhail et al., 1984; Snyder et al., 1982). The CH₂ Fermi resonance appears as a shoulder next to the CH₃ Fermi peak and could be located by the SFG data fitting as shown in the SI. Close inspection of Fig. 2a reveals that the dangling OH band decreased with time to negligible neglectable intensity after ~50 min under dark conditions. We have fitted the dangling OH band for at different times and present the results in Fig. S8-(Supporting Information) which clearly showing the decay of dangling OH intensity as a function of time. These changes reflect the adsorption rate and structuring of NA at the air-water interface at pH 8, which are accompanied by a slight increase of the OH bands at ~3450 cm⁻¹ and ~32<u>5</u>40 cm⁻¹ from interfacial water (Fig. 2a and Fig. S9), indicating a relatively slow restructuring of water molecules at the interface. At the same time, the CH₃-SS peak intensity, which we assume to be proportional to the number of interfacial NA, slightly increases with time when the sample was kept in the dark (see Fig. S10). The trivial small changes increase in the CH bands are expected due to ongoing interface adsorption until equilibrium is reached with full surface coverage and is not expected to be caused by photochemistry as all the experiments with the mixture so far were performed under dark conditions.

Although it was confirmed that 4-BBA partitions to the surface in the presence of NA (Tinel et al., 2016), no significant spectral signature of 4-BBA is observed at the air—mixture interface. Only a very week narrow band at ~3070 cm⁻¹, which can be ascribed to a =C-H stretch in an aromatic compound (Gautam et al., 2000; Hardt et al., 2024), could be identified after the data fitting of the dark spectrum of the mixture, Fig. S11a for pH8 and S11c for pH 5.4. We attribute this negligible contribution to the dominant presence of NA forming the top layer, hindering the 4-BBA from directly interfacing with air, limiting its contribution to surface signal, particularly since 4-BBA itself is not inherently surface-active.

Figure 2b shows SFG spectra at <u>air-water interface</u> interface for the mixture <u>at pH 8</u> which <u>were-was</u> first equilibrated for 80 min in dark and, then, exposed for different times to AM0 irradiation. There are two observed phenomena: 1) The <u>A significant increase in the appearance of a newaromatic band at 3070 cm⁻¹ as identified from the data fitting, Fig. S11b. (Gautam et al., 2000; Hardt et al., 2024) narrow band at ~3070 cm⁻¹ which can be ascribed to a =C H stretch in an aromatic compound (Gautam et al., 2000; Hardt et al., 2024)2) A bidirectional change, decrease and then increase, in the peak intensity of the water all bands as identified directly from the spectra. This The later means that two opposing processes occur simultaneously at the interface, as illustrated in the Discussion section. The appearance of the new band is expected and can be attributed to the photochemistry taking place at the water surface. However, the behavior of the water bands is questioned.</u>



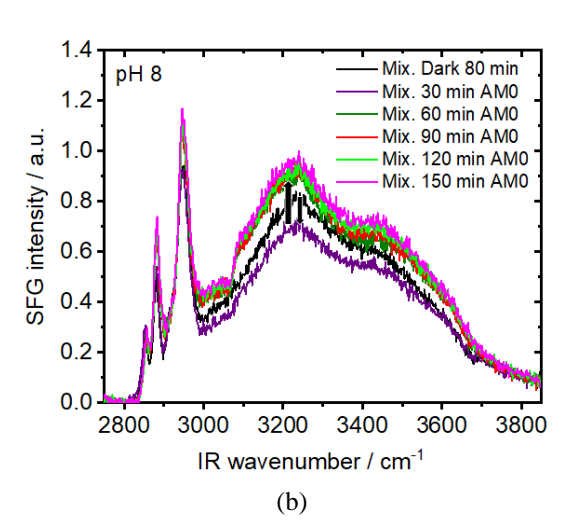


Figure 2: Changes of SFG spectra at <u>nir-waterair-water</u> interface of a 2 mM NA mixture with 0.2 mM 4-BBA at pH 8 as a function of time under (a) dark conditions as well as for (b) irradiation with AM0.

One possible reason for the anomalous bidirectional amplitude changes of the water bands under light conditions, as well as the slight change under dark conditions, is the change of pH of the bulk solution. Indeed, we found that the pH decreases with time for the same mixture under dark and light (UV) conditions until the pH stabilizes around a neutral pH, Fig. S12S13a. Under dark conditions, the

solution's pH decreases exponentially with time, however, under irradiation conditions, the pH also decreases but with a higher rate, blue curve in Fig. S13a. The decrease in pH under dark conditions is simply due to the carbonation of the solution under room conditions as was observed for a pH 8 solution without the mixture, orange curve Fig. S12S13a. The enhanced decrease in pH upon UV irradiation is only observed at pH 8 of the mixture solution which indicates a contribution from the reaction products. On one side, the water molecules at the surface are directly affected by the surface charge (Nihonyanagi et al., 2013). On the other side, the change in bulk pH changes the concentration dissociation fraction of the NA, Fig. S13b, and accordingly its concentration at the surface which in turn indirectly affects the water structuring and hence the SFG signal. The influence of pH on the detected SFG signal is described in details in the SI (section S4) will be discussed in the Discussion section.

To eliminate the complexity of pH effect and to reduce the number of variables, we examined the same system but at a moderate slightly lower pH value (pH = 5.4-5 to 5.6± 0.1) which is not very sensitive to carbonation and other factors that may change the pH value over time (green curve Fig. S12S13a). Indeed, the behavior of water bands (increase under dark conditions and decrease and then increase under light conditions) was not observed for low pH solution, Fig. 3b. In addition, the dangling OH, which characterizes the neat air waterair—water interface, was not observed at low pH in the first dark measurement, Fig. 3a. This means that the spread of NA on the surface was faster than that in the case of high pH. This is in line with the dependency of the dissociation constant of NA on pH. At intermediate pH, a considerable portion of negatively charged molecules are neutralized to create neutral fatty acid molecules, which have a much greater adsorption constant than their anionic counterparts (Badban et al., 2017). The aromatic CH stretching band at ~3070 cm⁻¹ was visible in the SFG spectrum after 60 min which is about the same time when it appeared for solution with pH 8 (Fig. 2b). However, the data fitting, shows that the aromatic band, for both pH values, started to increase directly after starting irradiations (Fig. 4b).

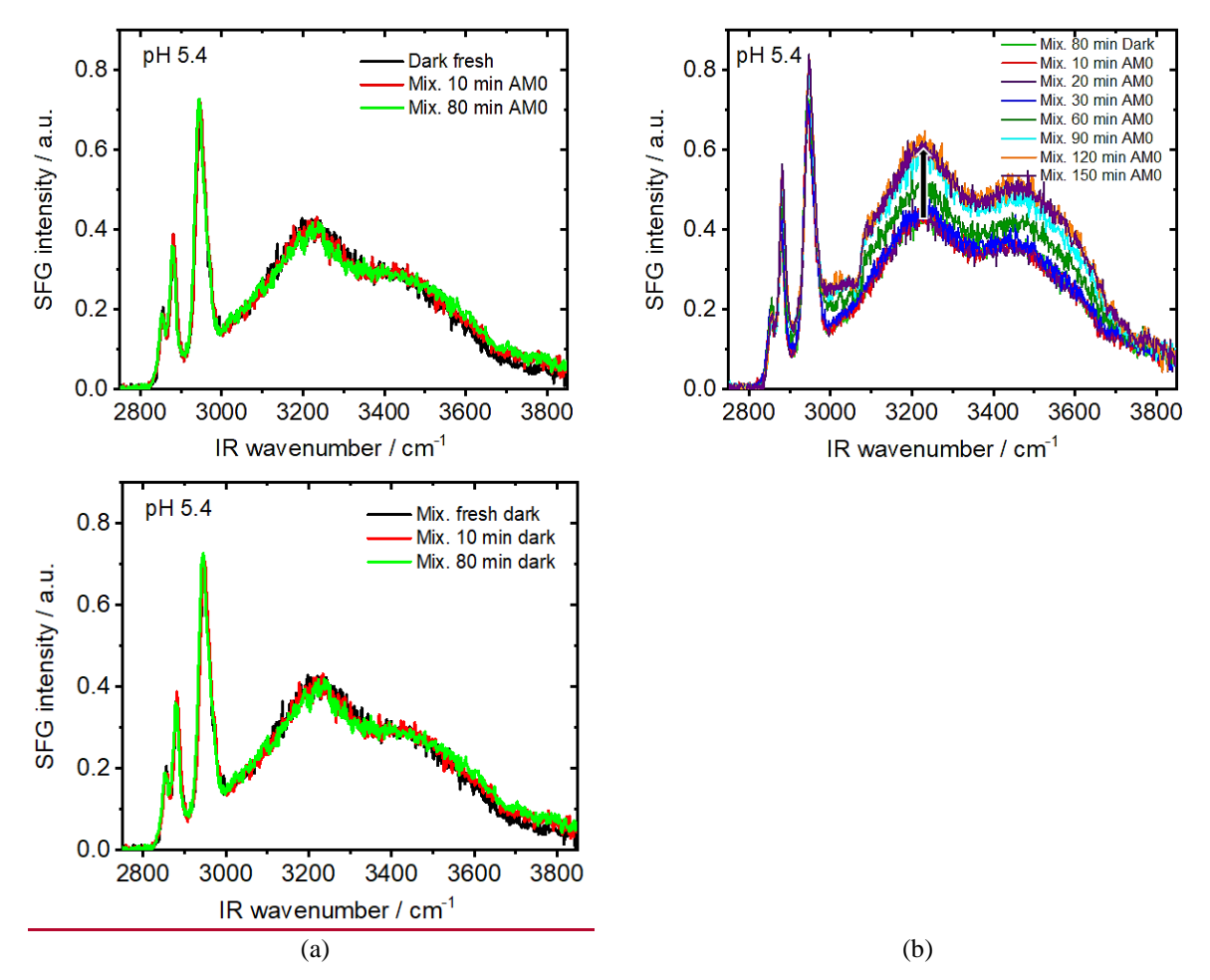


Figure: 3.SFG spectra at $\frac{\text{air-water}}{\text{air-water}}$ interface of the mixture, (2 mM NA + 0.2 mM 4-BBA) at pH5.4, under dark (a) and irradiation with AM0 (b) conditions.

The slight changes in the CH bands (2800 cm⁻¹ - 3000 cm⁻¹ region) indicate variations of the chemical composition in the topmost layer at the air—water interface. The significant increase in the aromatic band (~3070 cm⁻¹) indicates the formation of surface-active aromatic compound(s). The OH stretching modes in the 3100 cm⁻¹ – 3500 cm⁻¹ region, associated with interfacial water, increased after irradiation with AM0 (see the fitted spectra in Fig. S11). There is a clear proportion between the increase of the water band with the aromatic band, Fig. 4a. We attribute this to the formation of amphipathic aromatic compounds after irradiation, which can alter the hydrogen-bonding structure of water at the interface. Since SFG spectroscopy is inherently sensitive to the net polar orientation of interfacial molecules detecting vibrational modes only when molecular ordering breaks inversion symmetry, an increase in the SFG signal of hydrogen-bonded OH stretches indicates that water molecules at the interface have adopted a more ordered, non-centrosymmetric arrangement. This provides evidence for the presence of amphipathic species at the air—water interface, which promote directional hydrogen bonding via their polar headgroups. As a result, interfacial water molecules become more aligned, breaking the random symmetry of bulk water, orienting OH dipoles, and enhancing the net polar order, manifested as an increased SFG signal in the OH stretching region

(Gragson and Richmond, 1998; Kusaka et al., 2018)—. A direct comparison between the fitted amplitudes of the aromatic band (~3070 cm⁻¹) for pH 5.4 and pH 8 mixtures, Fig. 4b, shows a greater relative increase at pH 5.4, indicating a more favorable environment for the formation of the corresponding amphipathic aromatic compound. We attribute this tendency to the excess of hydrogen ions at lower pH which can be abstracted by the photoexcited 4-BBA resulting in the formation of C₁₄H₁₁O₃• radical in the solution (Eq. 1). This radical play an important role in the consequent reactions shown in the Tentative Reaction Pathways section.

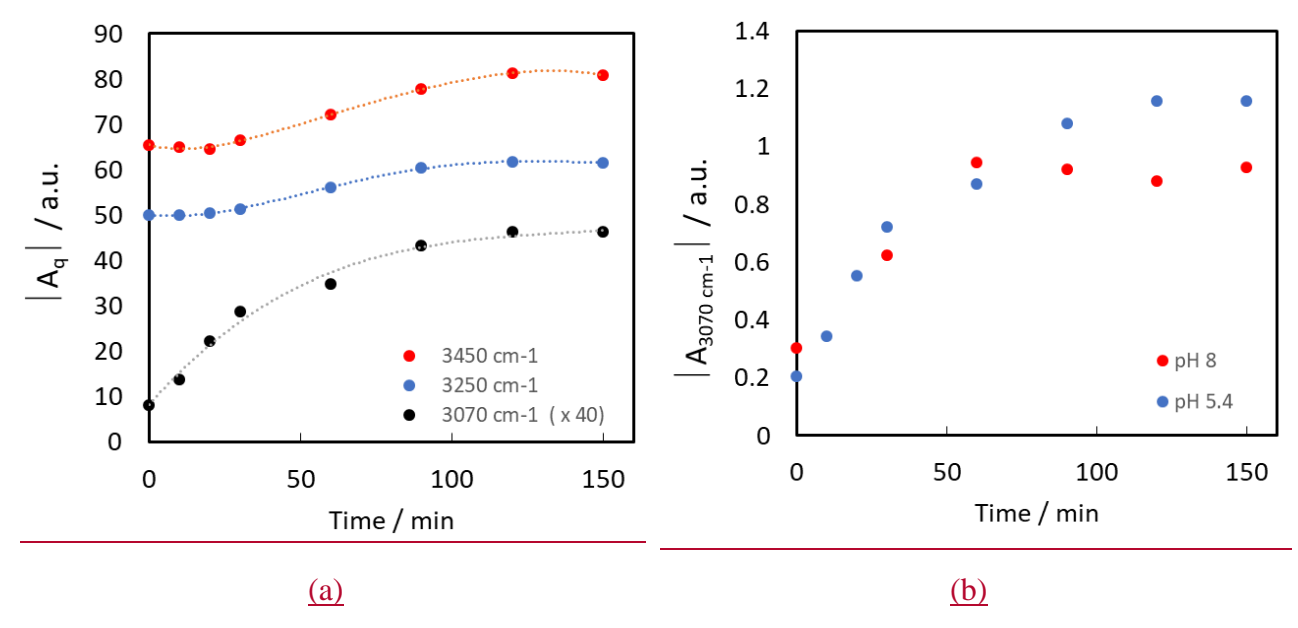


Figure 4: Time-dependent changes in the fitted SFG peak amplitudes with AM0 irradiation. (a) The aromatic band (~3070 cm⁻¹) and the two water bands (~3250 cm⁻¹ and ~3450 cm⁻¹) for the mixture at pH 5.4 (Dashed lines are included as visual guides). (b) The aromatic band (~3070 cm⁻¹) for the mixtures at pH 5.4 and pH 8.

The real solar radiation spectrum depends on weather, latitude, altitude and season. These factors qualitatively and quantitatively affect the photochemistry in the hydrosphere. In Fig. 5, To quantify the influence of the solar radiation spectrum on the photo reaction, we probed compare the effect of three irradiation conditions; AM0, AM1—(spectrum of solar light after traveling through the atmosphere), and solely the UV portion (λ < 400 nm) of AM0_for 90 min on the same mixture. The SFG spectra show strong variations after continuous irradiation with AM0 for 90 min, Fig. 5a. In contrast, the solution exposed to AM1 shows little presence of an aromatic band and a slight increase in water bands after the same irradiation time, Fig. 5b, which is in line with the reduced intensities of all spectral wavelengths, particularly the UV portion. The results in Fig. 4a show that the solution exposed to AM0 exhibited a strong aromatic band and a noticeable increase in water bands within one and a half hours. In contrast, the solution exposed to AM1 shows very little presence of an aromatic band and a slight increase in water bands after the same irradiation time, Fig. 4b. Irradiating the solutions with only the UV part of AM0 shows a clear aromatic band with almost no change in

the water bands, Fig. 4c. Irradiating the mixture with only the UV portion of AM0 (λ < 400 nm) shows a clear aromatic band with minimal changes in the water bands, Fig. 5c. This provides an evidence that the UV contribution plays a primary role in the formation of the surface-active aromatic compounds. Consequently, this photoreaction is likely more pronounced in the atmosphere (e.g. in cloud droplets) than at the sea surface where the UV intensity below 300 nm is very weak (see Fig. S4).

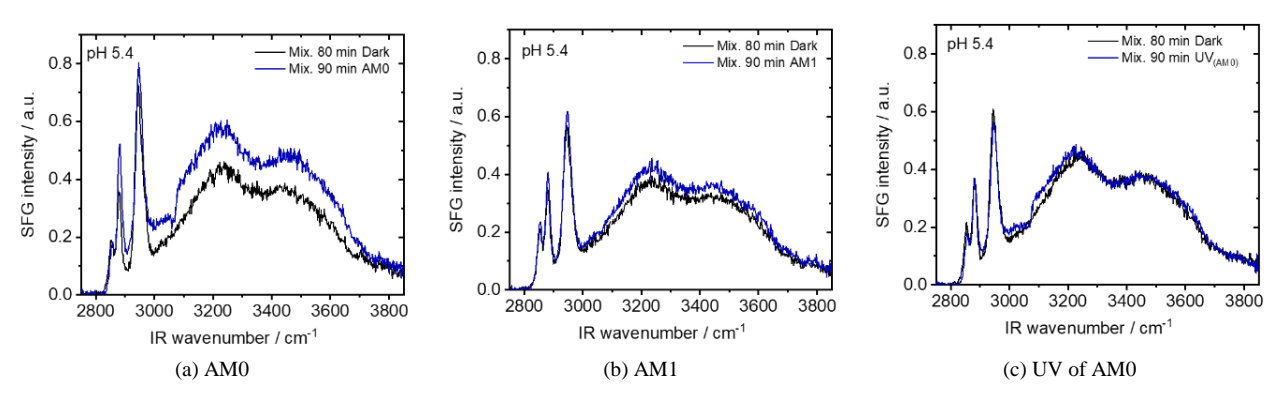


Figure 45: SFG spectra at air-water interface of 2 mM NA aqueous mixtures with 0.2 mM 4-BBA at a pH of 5.4, before and after irradiation with (a) AM0, (b) AM1 and (c) UV part-portion of AM0.

Finally, sSolutions at pH 5.6 were irradiated by ten different wavelengths for the same time (18 h) and an SFG spectrum was collected for the fresh solution, then after 0.5, 3 and 18 h of irradiation time. The intensity of each wavelength was adjusted to be equivalent to that of the corresponding wavelength in the AMO spectrum. Each irradiation wavelength was individually adjusted to match the corresponding intensity in the AMO solar spectrum, so that in separate irradiation experiments, each wavelength independently reflected its relative contribution to the AMO spectral power. The SFG spectra are shown in Fig. 5-6 and Fig. S11S12. Both figures correspond to the same set of measurements, but with different display formats to illustrate the change in the aromatic band and the changes in water bands respectively. Figure 5-6 shows that the aromatic band was considerably visible in the SFG spectrum, without data fitting (see black arrows), only in the short UV wavelengths, mainly 280, 310, and 345 nm, confirming the responsibility of the UV portion of the light for the generation of the aromatic compound(s). The effect of different wavelengths has different weights due to the changes in intensity and wavelength simultaneously. The shorter wavelength and/or higher intensity have a stronger effect on both the surface-active and bulk Fospecies. For the sample irradiated by 280 nm, the aromatic band was visible already after three hours although it has the lowest intensity in the solar irradiation spectrum. Figure \$\frac{\text{S11}}{\text{S12}}\$ shows that the water bands were changing differently with different wavelengths. The spectrum after 0.5 h has been omitted from Fig. \$11 for clarity reasons. In most of cases, the change in the aromatic CH stretching band was stronger at shorter wavelengths. The general trend of the band amplitudes looks almost similar but with faster changes at shorter wavelengths. However, in some cases it is different. For example, tThe solution irradiated with 365 nm shows a change in the water band after three hours similar to that of the solution irradiated with 280 nm. Except for the 280-310 nm, there is always an decrease increase or negligible change in the water bands after (at three hours) of irradiation. Except for 280 nm and 310 nm, the water bands after and then an increase (at 18 h of irradiation showed a minimum) in the water bands with irradiation. These variations in the water bands indicate changes in the hydrogen bonding structure at the interface due to the composition and abundance of the different photoproducts with different irradiations. Most likely the solution irradiated with 280 nm went through the same reaction path as for the other wavelengths but at an earlier time because of a faster photoreaction rate. The individual irradiation wavelengths have both different wavelengths and intensities which was done on purpose to mimic the corresponding solar irradiance for each wavelength. The SFG study also showed that the salt concentration of the bulk accelerates the photo reaction (see Sect. S5 and Fig. S14). It is not the focus of this paper to discuss the details of the salinity effect on the photochemistry at this surface, we only register the observed phenomenon. The results highlight the complex impact of solar spectrum composition on reaction pathways. They also emphasize the importance of incorporating these variations into the photochemical models used in atmospheric science for more accurate predictions of the complex chemical interactions that occur in the atmosphere (Xing et al., 2022). (Xing et al., 2022).

1

2

3

4

5

6

7

8

9

10

11

12

13

14

15

16

17

18

19

20

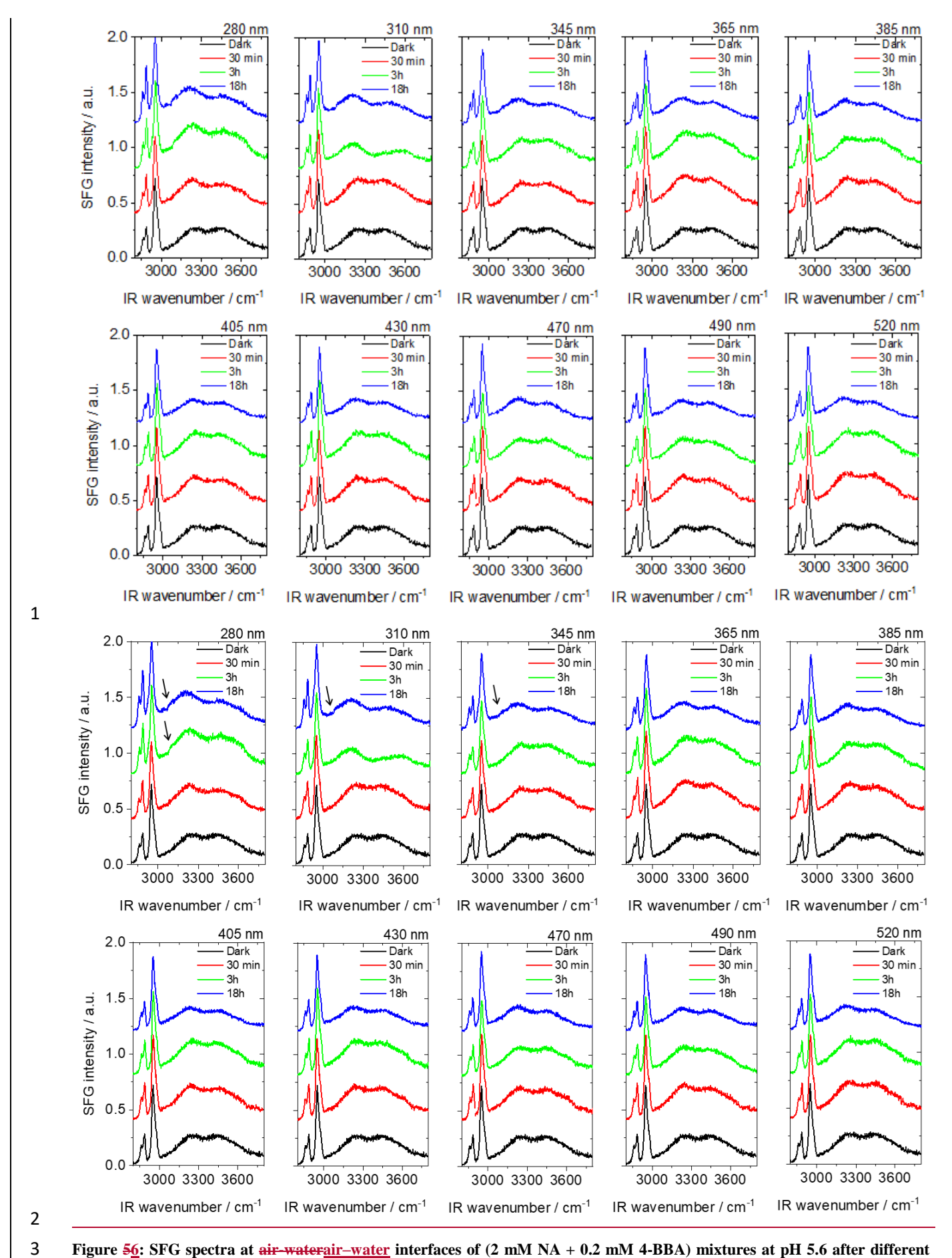


Figure $\frac{56}{2}$: SFG spectra at $\frac{1}{2}$ spectra at $\frac{1}{2}$ interfaces of (2 mM NA + 0.2 mM 4-BBA) mixtures at pH 5.6 after different times of irradiation with different wavelengths. Note that the spectra have a constant with offset.

Finally, although it is not intended to investigate the salinity effect on the photochemistry at the surface in this study, we report on its potential influence on the photoreaction of the NA-4BBA system. SFG pilot experiment showed that the salt concentration of the bulk accelerates the photo reaction (see section. S5 and Fig. S15). We only register the observed phenomenon and aim at detailed study in future work.

1 3.2 Organic compounds in Chemical composition of liquid and gas and liquid

2 phase

The aromatic compound detected at the air-waterair-water interface by SFG spectroscopy is a result of a photoreaction occurring for the studied samples when they are irradiated with UV containing radiation e.g. AM0. As previously mentioned, this surface active compound and the minute details on pH effect and water band changes were not reported by the linear techniques used in the reference work by Tinel et al., 2016. The reactions in the visible wavelength range were neither expected nor previously reported. Considering these facts and recalling that the mass spectroscopic results in Tinel et al., (2016) (Tinel et al., 2016), although very thorough, were collected from samples irradiated with a commercial Xenon lamp as a light source, and that the 4-BBA sample was not purified as ours, we decided to repeat the mass spectrometry measurements using our solar simulator and purified 4-BBA samples (see experimental details).

3.2.1 Aqueous phase analysis

1

2

3

4

5

6

7

8

9

10

11

12

13

14

15

16

17

18

19

20

21

22 23

24

25

26

The products of the photochemical reactions of NA in the presence of 4-BBA were detected under different irradiation and at a fixed pH of ~5.8. Figure 6-7 shows the evolution of seven main liquidphase products detected in experiment MS.1 under irradiation with AMO and in the presence of 4-BBA as photosensitizer with the following sum formulas: C₈H₁₂O₄, C₈H₁₂O₅, C₉H₁₀O₅, C₉H₁₄O₃, C₉H₁₆O₃, C₉H₁₆O₄, and C₁₀H₁₄O₄. Among the photoproducts identified in the liquid phase, only C₉H₁₆O₃ and C₉H₁₆O₄ were also reported in the reference study (see table S4). Conversely, the reference study reported additional products that were not detected in our analysis (see table S6). This could be attributed to the purity of the sample, the spectral intensity distribution of the light source and/or the different analytical instrumentation as mentioned in the experimental section. The suggested assignments of the detected compounds in the liquid phase are listed in Table S4 of the Supporting Information SI. Some of the products showed faster production rates during the first hour, while the others showed a slower rate. We do not observe any correlation between the production rate and chain length nor the molecular weight. However, the differences are close to the experimental uncertainties. The sum of all C_xH_yO_z signal intensities in the liquid phase shows a linear relation with the time of irradiation, Fig. 67. Figure 7-8 shows the ratio of signals detected for the main liquidphase photoproducts of the mixture (NA + 4-BBA) versus the signals detected in the absence of 4-BBA with irradiation of AMO and in the presence of synthetic air. The results show the largest promotion in the formation of C₈H₁₂O₄, C₉H₁₀O₅ and C₉H₁₆O₃ in the presence of 4-BBA.

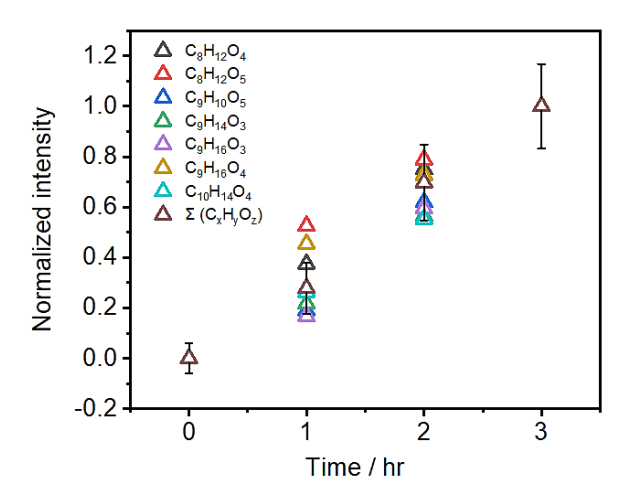


Figure 67: Intensities Concentrations of each individual photoproducts as a function of exposure times to AM0 irradiation (Exp. MS.1), normalized to the total liquid-phase signal intensity sum the of all products $\Sigma(C_xH_yO_z)$ -signal intensities in the liquid phase. Error bars represent the uncertainty associated with the analytical measurements.

To examine the role of oxygen in the reactions, we repeated the AM0 experiment with pure nitrogen, instead of the synthetic air, and deoxygenated liquid solutions (Exp. MS.3). The solution was deoxygenated by bubbling with nitrogen for 10 min and the measuring cell was purged before closing it hermetically. Figure 8-9 shows the ratio of signals detected in the presence of synthetic air versus those in the presence of N_2 . The results show that the presence of oxygen causes an increase of $C_8H_{12}O_5$, $C_9H_{14}O_3$, $C_9H_{16}O_3$, and $C_9H_{16}O_4$ by a factor of 10 to 12. The presence of oxygen shows only a limited promotion on the formation of $C_8H_{12}O_4$ (factor of ~2), but a significant promotion on the formation of $C_{10}H_{14}O_4$ (factor of ~19) and $C_9H_{10}O_5$ (factor of ~34). This emphasizes the vital role of dissolved oxygen in the natural bodies of water to develop multiple pathways of interactions.

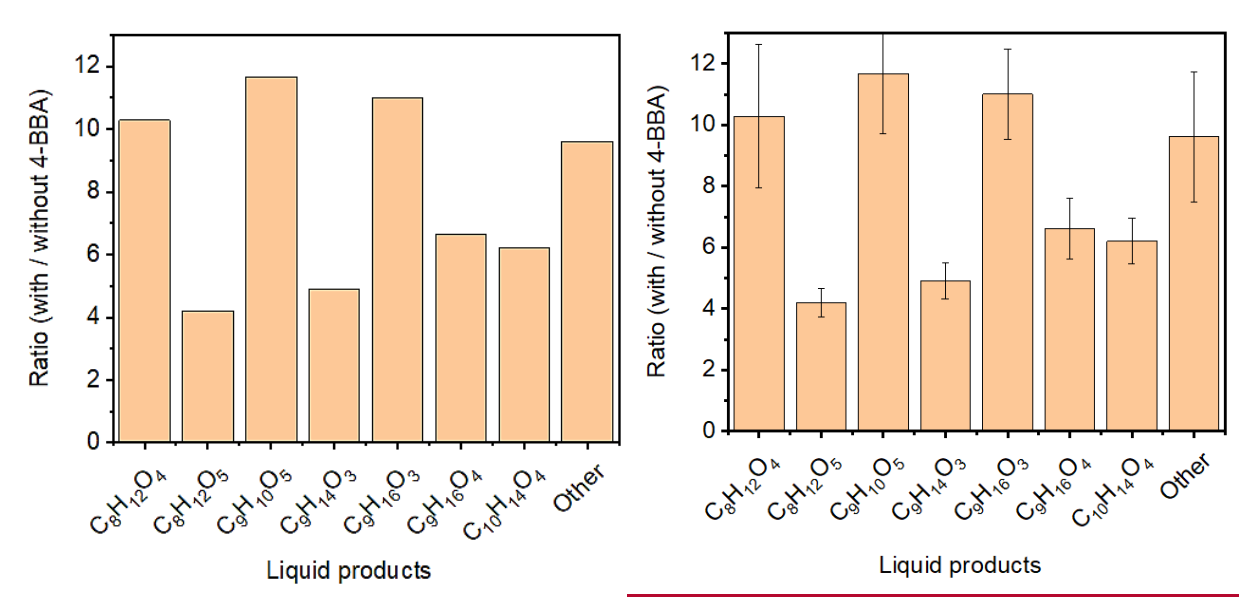
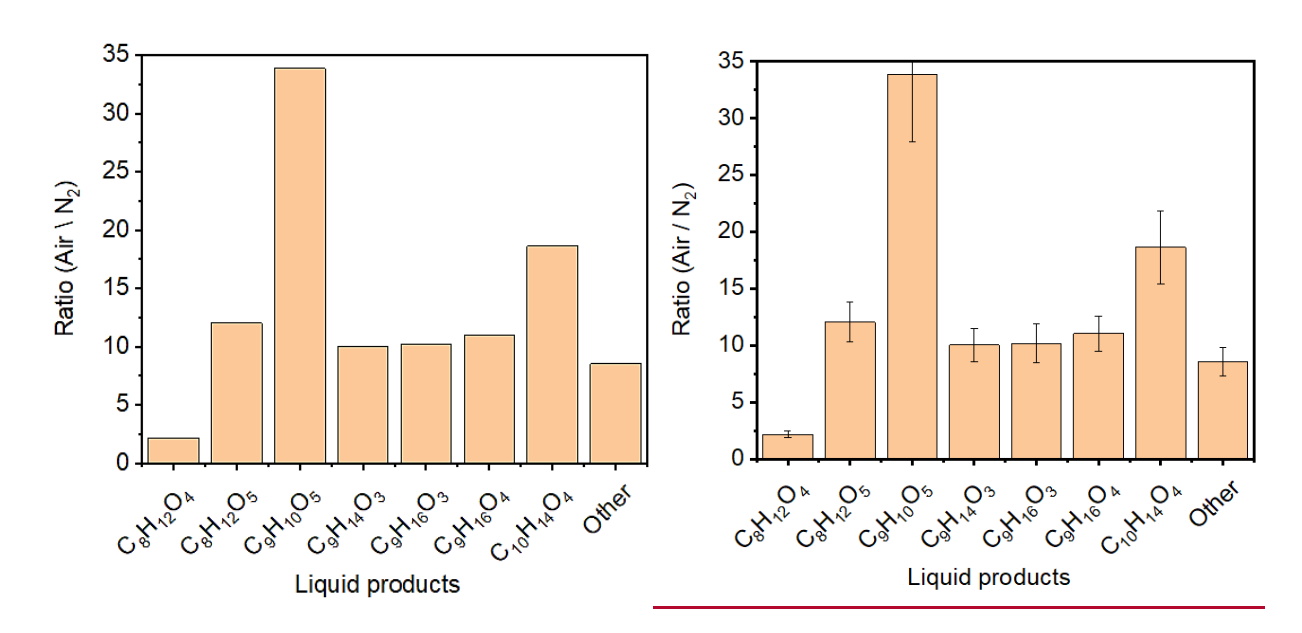


Figure 78: Ratio of the signal detected in the presence of 4-BBA to that the signal observed without 4-BBA for the main detected photoproducts detected in the aqueous phase for an aqueous solution with of NA solution with irradiated without AM0 for three hours under in a synthetic air environment.



2

3

4

5

6

7

8

9

10

11

12

13 14

15

16

17

18

19

20

21

22

23

24

25

Figure 89: Ratio of the signal detected in the presence of 4-BBA and synthetic air environment compared to those that in the absence of oxygen in gas and liquid phase for the main photoproducts detected in the aqueous phase of NA with 4-BBA, after irradiation with AMO for three hours.

The SFG spectra of solutions irradiated with different single wavelengths, Fig. 6, exhibited varying changes in the water bands regardless of the appearance of the aromatic CH stretching band. To quantify the effect of different irradiation wavelengths on the generation of photoproducts, we further examined the solution mixture irradiated with sunlight and also with four selected single wavelengths in the UV and Visible part of the spectrum. Figure 10 shows the total C_xH_yO_z signal detected in the liquid phase for different irradiation conditions as illustrated at the x-axis. Finally, we compare the product formation under AMO and AM1 to that under sunlight. Figure 9-11 shows a comparison between the ratios of the photo-products for the mixtures irradiated with AM0 (Exp. MS.1) and with AM1 (Exp. MS.2) versus irradiation with real sun light, during a clear sunny day in Karlsruhe, Germany, on the, 1st June 2023 from 11 am to 2 pm (Exp. MS.8) versus irradiation with AM1 (Exp. MS.2). The day and time were chosen to guarantee minimal changes in the solar radiation spectrum. As can be inferred from Fig. 10, Withwith stronger UV light at AMO, the formation of major aqueous photoproducts was promoted, with the increase of total C_xH_yO_z signal by a factor of about 2.4 compared to that at AM1. After being irradiated by real solar light for three hours, the total C_xH_yO_z signal observed was ~0.9 of that observed at AM1. Hence, our experiments with AM1 irradiation are indeed comparable to typical atmospheric conditions at earth surface. The same main set of photoproducts observed under artificial irradiation in the laboratory were also detected under sunlight. After being irradiated by real solar light for three hours, the total C_{*}H₂O₂ signal observed was ~0.9

- 1 of that observed at AM1. Hence, our experiments with AM1 irradiation are indeed comparable to
- 2 typical atmospheric conditions at earth surface. The The relative product fractions for irradiation with
- 3 sunlight are very similar to those of the lab irradiation and mostly lie between those of irradiation by
- 4 AM0 and AM1. The fractions of the photoproducts that constitute of 2 % or more of the total products
- 5 under real sunlight (i.e. C₉H₁₆O₄, C₁₀H₁₄O₄, C₈H₁₂O₄, C₉H₁₆O₃, and C₉H₁₀O₅, in order of ascending
- 6 fraction—was all and emphasisemphasizes the
- 7 capability of our homemade light source to simulate ambient solar radiation.

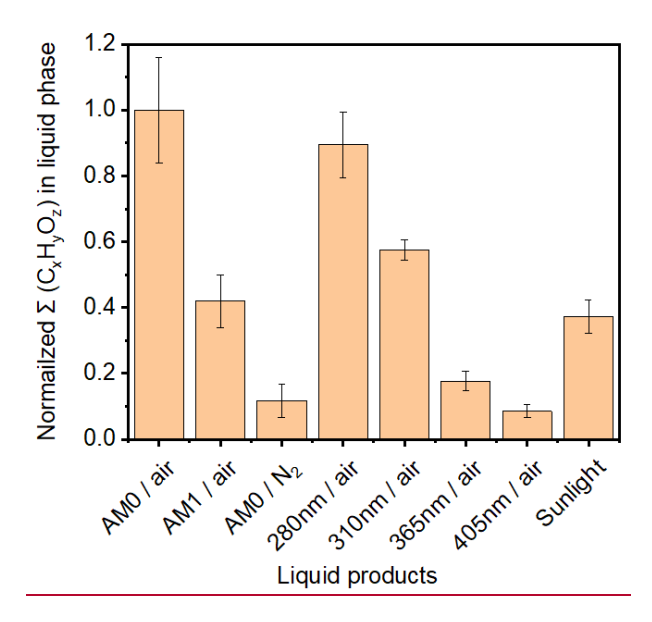


Figure 10: Normalized total $C_xH_yO_z$ signal in aqueous phase at different irradiation conditions for three hours. [Exps. MS.1 to MS.9 (SI)]

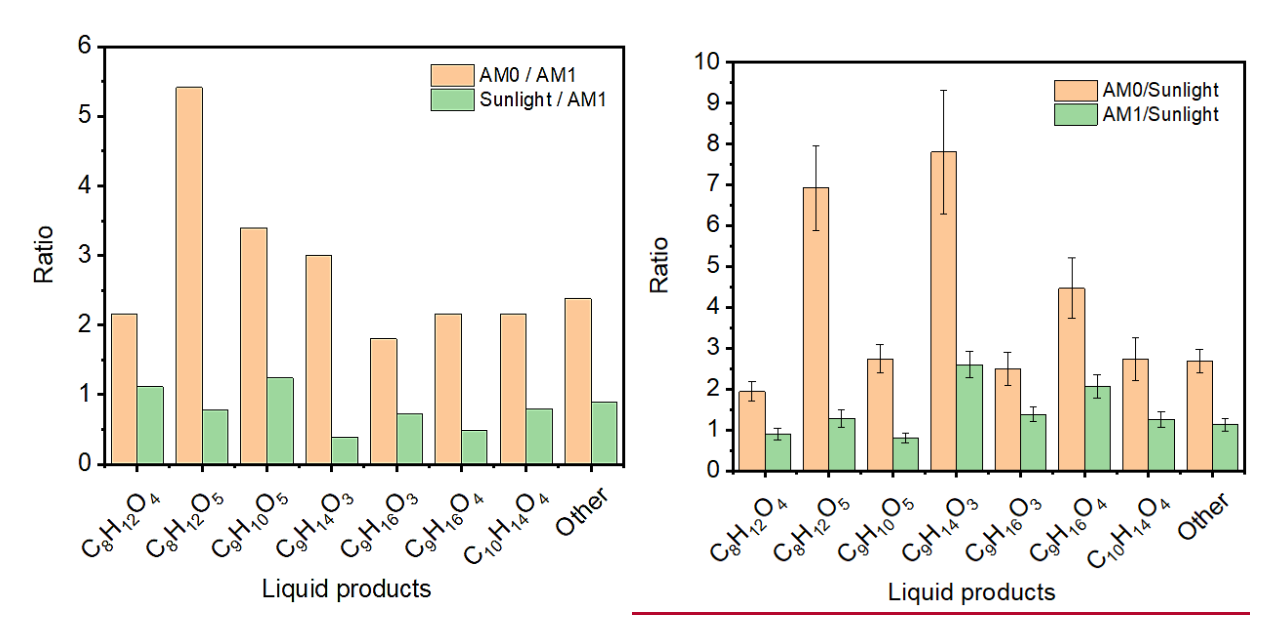


Figure 911: Ratio of the compounds detected with AM0 or sunlight versus the signal with AM1 versus the signal with sunlight, for a NA aqueous solution with 4-BBA after irradiation for three hours.

The SFG spectra of solutions irradiated with different single wavelengths, Fig. 5, exhibited varying changes in the water bands regardless of the appearance of the aromatic CH stretching band. To precisely quantify the effect of different irradiation wavelengths on the generation of photoproducts, we examined the solution mixture irradiated with four selected single wavelengths in the UV and Visible part of the spectrum. Figure 10 shows the total C_xH_yO_z signal detected in the liquid phase for different irradiation conditions as illustrated under the x-axis.

- 1 To address the wavelength dependence of the photoproducts further, we plot the fraction of the three
- 2 most dominating products, namely $C_8H_{12}O_4$, $C_9H_{10}O_5$, and $C_9H_{16}O_3$, versus irradiation wavelength in
- 3 Fig. $\frac{11}{12}$. The fractions of $C_8H_{12}O_4$ and $C_9H_{16}O_3$ increase with longer wavelength while the fraction
- 4 of the C₉H₁₀O₅ increases with shorter wavelength indicating two different mechanisms as will be
- 5 described in the discussion section below.

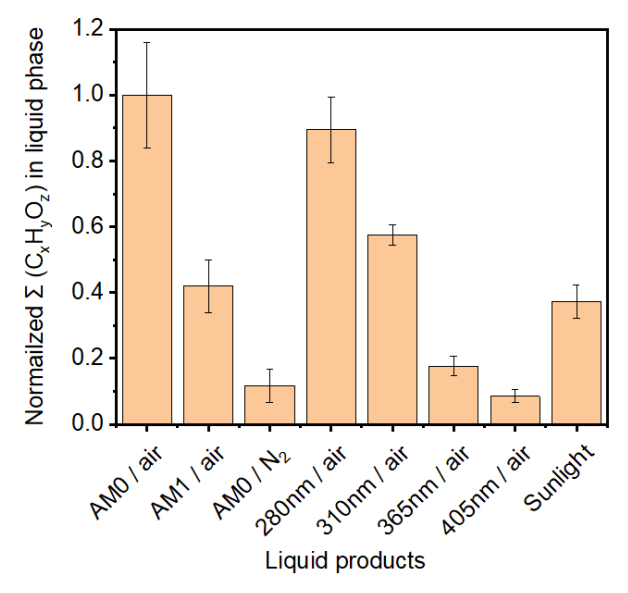


Figure 10: Normalized total C_xH_yO_x signal in aqueous phase at different irradiation conditions. [Exps. MS.1 to MS.9 (SI)]

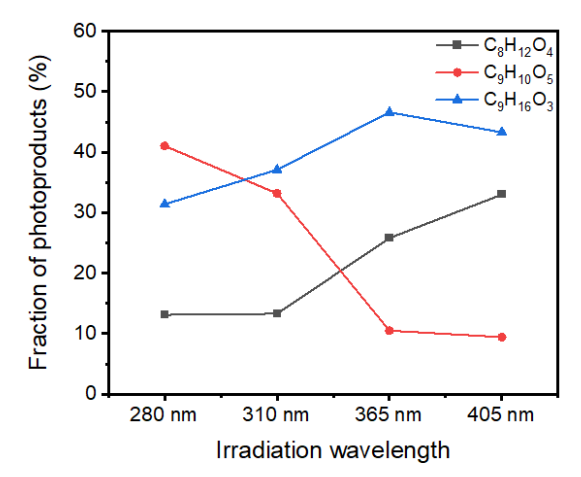


Figure $\frac{1112}{1}$: The fraction of photoproducts versus wavelength for the three most dominating products, $(C_8H_{12}O_4, C_9H_{10}O_5, and C_9H_{16}O_3)$ in a NA aqueous solution with 4-BBA after irradiation with 280, 310, 365, and 405 nm for three hours.

In all MS experiments, $C_8H_{12}O_4$, $C_9H_{10}O_5$, and $C_9H_{16}O_3$ were the most abundant products detected in the liquid phase. However, the fractions of the liquid-phase compounds varied under different irradiation conditions, Fig. 13a to h. The $C_8H_{12}O_4$ is a major product from the photoreaction of NA with limited dependence on oxygen compared to other products. This is evident from the increase of the fraction of $C_8H_{12}O_4$ in total liquid-phase $C_xH_yO_z$ in experiment in pure nitrogen, Fig. 13c. The formation of $C_8H_{12}O_4$ was also significantly increased in the presence of 4-BBA, Fig. 8, indicating that $C_8H_{12}O_4$ was a photodegradation product from NA in the presence of 4-BBA. For $C_9H_{16}O_3$, which is suggested to form through RO_2 radical reactions after hydrogen abstraction on (Tinel et al., 2016)NA (Tinel et al., 2016), its fraction of total liquid-phase $C_xH_yO_z$ was higher with irradiation of AM1 than AM0 Fig. 13b and a, respectively. This stands in agreement with the measurement with irradiation from 280 nm to 405 nm, Fig. 13e to h. With more UV at 280 nm and 310 nm, $C_9H_{16}O_3$ accounted for about ~31 % and ~37 % of total $C_xH_yO_z$, respectively; while with less UV at 365 nm and 405 nm, the fractions of $C_9H_{16}O_3$ increased to ~47 % and ~43 %, respectively. In previous work

by Tinel et al. (2016)-(Tinel et al., 2016), the solution with NA and 4-BBA showed that the formation 1 2 of C₉H₁₆O₃ increased by a factor of ~2.5 in the presence of air. In our study, with 4-BBA the formation of C₉H₁₆O₃ increased by a factor of ~11. The oxygenated C₉ products are promoted when O₂ is 3 abundant, which agrees with Tinel et al. (2016). (Tinel et al., 2016) In contrast to C₈H₁₂O₄ and 4 C₉H₁₆O₃, the fraction of C₉H₁₀O₅ in total liquid-phase C_xH_yO_z decreased from ~41 % at 280 nm to 5 6 ~9 % at 405 nm and also from ~34 % at AM0 to ~24 % at AM1. We observed a higher fraction of 7 C₉H₁₀O₅ in experiments involving NA and 4-BBA under enhanced UV conditions, suggesting that 8 C₉H₁₀O₅ is likely an aromatic compound formed through reactions between photoproducts generated from the photolysis of both NA and 4-BBA. This interpretation aligns with the presence of two 9 distinct reaction mechanisms, as inferred from Fig. 12, where 4-BBA functions both as a 10 photosensitizer for NA, producing nonaromatic products such as C₈H₁₂O₄ and C₉H₁₆O₃, and as a 11 photolabile compound that yields aromatic photoproducts which may undergo further reactions. 12

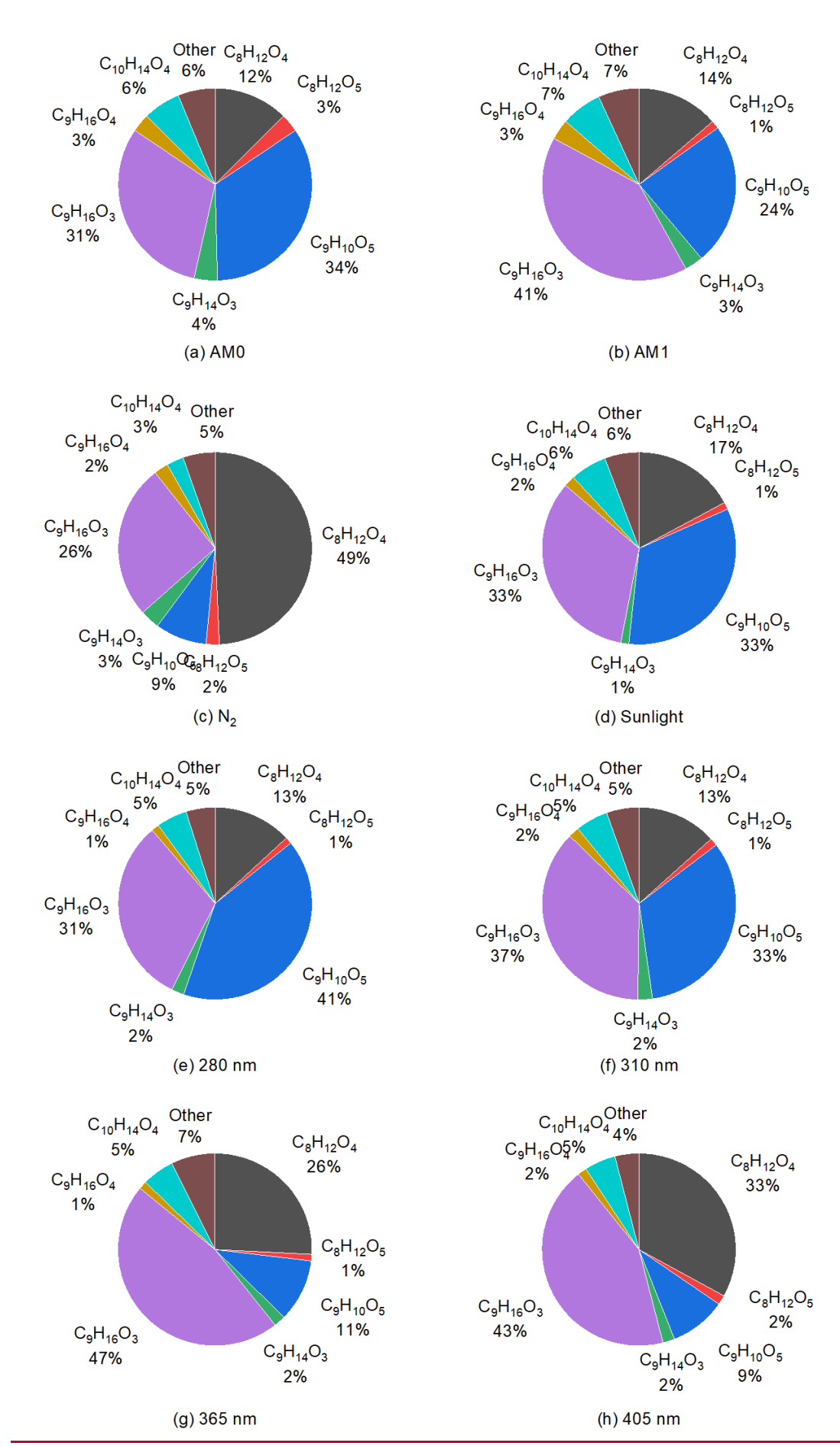


Figure 13: Fractions of products in total liquid-phase $C_xH_yO_z$ under different irradiation conditions. All panels represent experiments conducted in air, except panel (c), which corresponds to an experiment performed in pure nitrogen.

$4BBA(C_{14}H_{10}O_3) * \xrightarrow{hv} C_{14}H_{11}O_3 .$	<u>+</u>
$C_{14}H_{11}O_3 \cdot + H \cdot \xrightarrow{hv \leq 310 \ nm} C_6H_6 + C_8H_5O_3 \cdot$	(II)
$4BBA(C_{14}H_{10}O_3)*+C_9H_{18}O_2 \xrightarrow{hv} C_{14}H_{11}O_3 \cdot +C_9H_{17}O_2 \cdot$	(III)
$C_{\mathfrak{g}}H_{17}O_{2} \xrightarrow{O_{2}} C_{\mathfrak{g}}H_{17}O_{4} \cdot$	(IV)
$C_9H_{17}O_4 \xrightarrow{RO_2} C_9H_{16}O_3 + C_9H_{18}O_3$	(V)
$\xrightarrow{C_9H_{17}O_4}\xrightarrow{O_2,HCO_3}C_{0,0}/C_{0,0}$	(VI)
$C_9 H_{16} O_3 \xrightarrow{hv, OH} C_9 H_{14} O_3 + C_9 H_{16} O_4$	(VII)
$C_{14}H_{11}O_3 \cdot + C_9H_{17}O_4 \cdot \rightarrow C_{23}H_{28}O_7$	10111
$C_{23}H_{28}O_{7} \rightarrow C_{9}H_{10}O_{5} + C_{14}H_{18}O_{2}$	(IX)

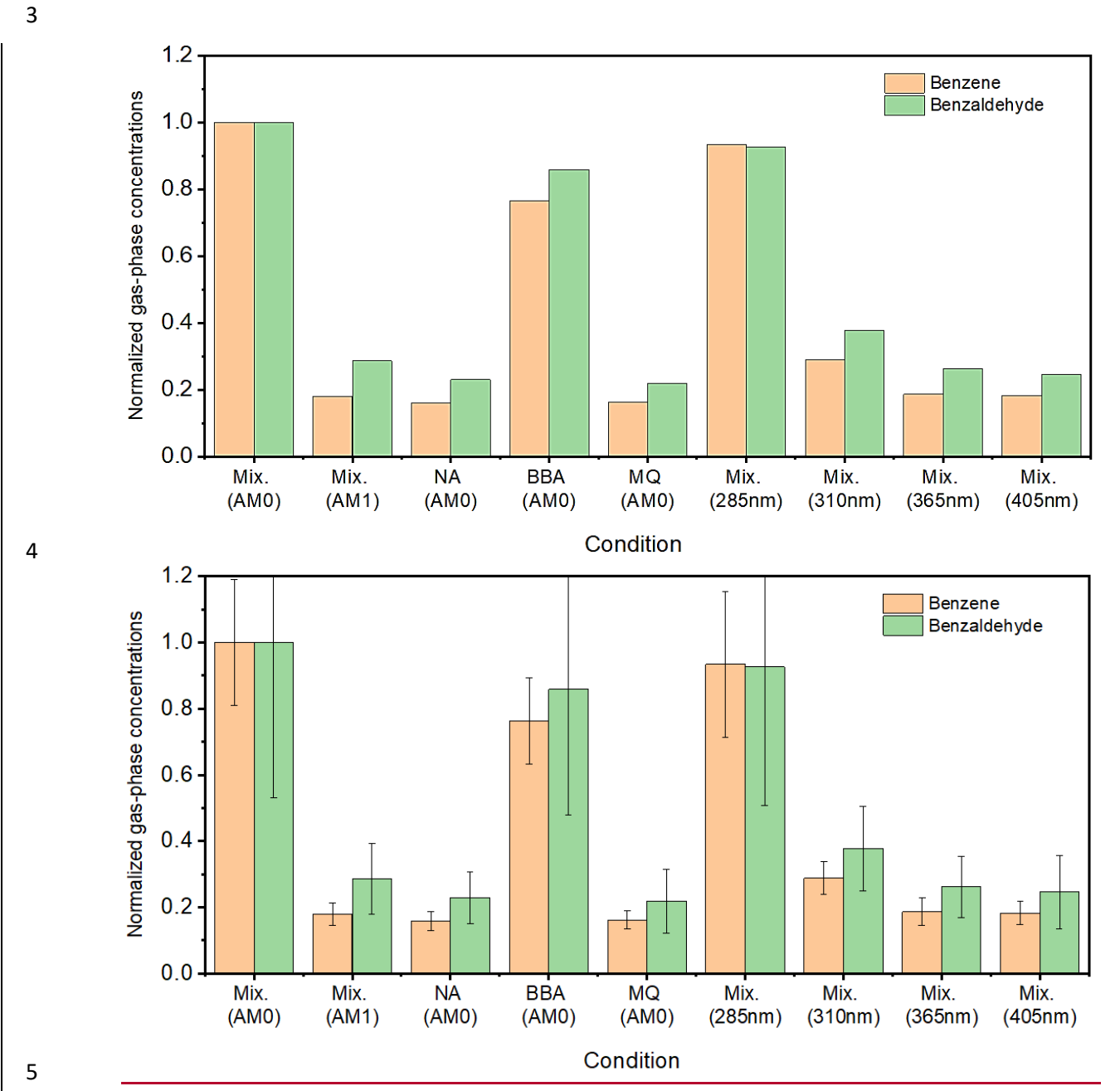
3.2.2 Gas phase analysis

1

2

Examining the gas phase is important to detect the volatile photoproducts. A series of compounds, 3 such as C₄H₈ (butene), C₄H₈O (butanal), C₅H₁₀ (pentene), C₅H₁₀O (pentanal), C₆H₆ (benzene), C₇H₈ 4 5 (toluene), C₇H₆O (benzaldehyde), C₈H₁₆O (octanal), as well as some undefined fragments such as C₆H₅ and C₇H₆ were detected in the gas phase (see Table S5). Similar to the liquid phase, only a 6 7 subset of the photoproducts identified in the gas phase, namely C_4H_8 , C_4H_8O , $C_5H_{10}O$, and 8 C₈H₁₆O were also reported in the reference study, which, in contrast, identified additional products 9 not observed in our analysis (see Table S6). Only two of the photoproducts detected in the gas phase which showed a significant increase 10 11 compared to the background experiments (BG1-3). Figure 12-14 shows the normalized signals of the two main gas-phase compounds: benzene (C₆H₆) and benzaldehyde (C₇H₆O) under different 12 irradiation conditions. When NA was irradiated in the absence of 4-BBA, the signal from both 13 products remained at background levels. However, when either the mixture or 4-BBA alone was 14 15 irradiated with AMO, both compounds exhibited strong signals. This is a further confirmation elearly indicates that, in addition to the previously reported photosensitized degradationphotochemical 16 17 reaction of NA in the presence of 4-BBA as a photosensitizer, 4-BBA itself undergoes photolysis under the influence of the UV portion of the light spectrumirradiation. For other gas-phase 18

compounds detected in this study, no significant differences were observed between the normal irradiation experiments and the background experiments.



Figure— $12\underline{14}$: MS signals of benzene and benzaldehyde detected in the gas phase for different solutions under different irradiation conditions for three hours. Signals are normalized to that of the mixture under AM0 irradiation condition. \underline{MQ} : $\underline{Milli-Q}$ water (pH ~ 6.2).

3.2.3 Tentative reaction pathways

2 The following scheme shows the suggested photolysis of NA in the presence of 4-BBA:

3

$$4BBA(C_{14}H_{10}O_3) \stackrel{hv}{*} C_{14}H_{11}O_3 . \tag{1}$$

$$C_{14}H_{11}O_3 \cdot + H \stackrel{hv \leq 310 \, nm}{\longrightarrow} C_6H_6 + C_8H_5O_3 \cdot$$
 (2)

$$4BBA(C_{14}H_{10}O_3)*+NA(C_9H_{18}O_2) \xrightarrow{hv} C_{14}H_{11}O_3 \cdot +C_9H_{17}O_2 \cdot \tag{3}$$

$$C_9H_{17}O_2 \stackrel{O_2}{\longrightarrow} C_9H_{17}O_4$$
 (4)

$$C_9H_{17}O_4 \xrightarrow{RO_2} C_9H_{16}O_3 + C_9H_{18}O_3$$
 (5)

$$C_9H_{17}O_4 \xrightarrow{O_2,HCO_3} C_{10}H_{14}O_4$$
 (6)

$$C_9H_{17}O_4 \cdot + C_{14}H_{11}O_3 \cdot \rightarrow C_{23}H_{28}O_7$$
 (7)

$$C_{23}H_{28}O_7 \rightarrow C_9H_{10}O_5 + C_{14}H_{18}O_2$$
 (8)

$$C_9H_{16}O_3 \xrightarrow{hv,OH} C_9H_{14}O_3 + C_9H_{16}O_4$$
 (9)

4

5 [Green are products detected by MS] [Ref?]

6 The photochemical degradation of NA in the presence of 4-BBA proceeds through a series of radical-7 mediated reactions. The proposed mechanism begins with the photoexcitation of 4-BBA generating 8 a reactive triplet state 4-BBA* (Dalton et al., 2025), which abstracts a hydrogen atom from either the 9 solvent or NA, generating C₁₄H₁₁O₃• (Eq-1) (Jiménez and Miranda, 2018). This radical undergoes 10 Norrish I-type cleavage to produce benzene (C_6H_6) and a benzoyl fragment ($C_8H_5O_3$ •) with UV 11 absorption at $\lambda \le 310$ nm (Eq-2) (Goswami et al., 1985). $C_8H_5O_3$ • may further react with O_2 to form oxygenated intermediates. In parallel, 4-BBA's triplet state interacts with NA, abstracting a hydrogen 12 13 atom to form a NA-derived alkyl radical (C₉H₁₇O₂•) (Eq-3), which reacts with oxygen to yield a peroxy radical (C₉H₁₇O₄•) (Eq-4) (Atkinson, 2000)-. Subsequent reactions of this peroxy radical 14 include: (1) reaction with other RO₂ forming C₉H₁₆O₃ and C₉H₁₈O₃ (Eq-5) (Freeman-Gallant et al., 15 2024), (2) oxidation with bicarbonate radicals (HCO₃•) [Ref] (Yan et al., 2019) to form C₁₀H₁₄O₄ 16 17 (Eq-6), and (3) cross-coupling with the 4-BBA ketyl radical ($C_{14}H_{11}O_{3}$) to produce an unstable adduct (C₂₃H₂₈O₇) (Eq-7), having peroxide bond (-O-O-) which is very reactive and unstable under 18 light (You et al., 2020). The unstable C₂₃H₂₈O₇ undergoes rapid intramolecular rearrangement and 19 fragmentation. It could fragment into the observed aromatic product C₉H₁₀O₅ and a NA-derived 20 21 byproduct (C₁₄H₁₈O₂) (Eq-8). C₉H₁₆O₃ may undergo photooxidation under UV light in the presence

of hydroxyl radicals, resulting in the formation of one oxidized product (C₉H₁₆O₄) and one dehydrogenated product (C₉H₁₄O₃), suggesting radical-mediated transformation (Eq-9) (Numadate et al., 2022). The C₉H₁₀O₅ product, observed in higher concentrations particularly after irradiation with AMO, can be formed in an amphipathic, aromatic, surface-active structure via peroxide intermediates that react with water and give OH-radicals (Kroll et al., 2015; Lankone et al., 2020). This product (C₉H₁₀O₅) gives rise to the SFG signal at 3070 cm⁻¹ and leads to the increase in the water bands in the region 3100 cm⁻¹ to 3500 cm⁻¹. Our proposed chemical structures with pathways can be seen in the SI, Fig. S16. Compared to the reaction path ways suggested by Tinel et al. 2016 (Tinel et al., 2016) our reactions involve the consequences of the photolysis of 4-BBA under the influence of the UV portion on the irradiation source.

4. Discussion

As previously mentioned the aim of this work was to explore on the molecular level the photochemistry of the organic surfactant NA at the air-water interface in the presence of the photosensitizer 4-BBA. For that, we have used environmental conditions that are similar to the real environment at sea water and droplets in the atmosphere. We examined three irradiation conditions which are equivalent to solar irradiation at the top of atmosphere and near the sea level. We have also examined pH values which are representative of most natural water bodies (~pH 6 to 8). In our study we utilized an LED solar simulator that produces a light spectrum that is closer to the solar spectrum than that of the Xenon lamp used in the reference work (Tinel et al.).

4.1 Influence of the irradiation spectrum

The real solar radiation spectrum depends on weather, latitude, altitude and season. These factors qualitatively and quantitatively affect the photochemistry in the hydrosphere. The irradiation of the mixture with AM0 which includes wavelengths lower than 310 nm yielded the largest quantity of surface and bulk phase photoproducts among all the experiments. SFG spectra presented above indicate strong signals at 3070 cm⁻¹ which are indicative for aromatic moieties at the air water interface formed after continuous irradiation with AM0 for 90 min (Fig. 4a). Changes in the CH bands also point to variations of the chemical composition in the topmost layer at the air water interface. In addition, also OH stretching modes from interfacial water increased significantly after irradiation with AM0. We propose that the latter is associated to the formation of hydrocarbons that can change the structure of hydrogen bonded water molecules at the interface upon their formation which is triggered by irradiation of the samples with e.g. AM0. Irradiation with AM1, Fig. 4b, showed a weaker effect compared to that after the irradiation with AM0 which is in line with the reduced intensities of all spectral wavelengths, particularly the UV part. However, experiments where the wavelength and/or the spectrum of the light irradiation was systematically varied provided evidence

that only the UV contribution to AM0, Fig. 4c, is responsible for the observed photochemical reaction of NA mixtures with 4-BBA. Particularly, aromatic products are produced in the presence of UV light by the photolysis of 4-BBA, as will be discussed in detail in the next section. This means that the main effect producing the aromatic compound comes from the UV part of the solar spectrum and such a photoproduct would be produced in the atmosphere (e.g. in cloud droplets) rather than at the sea surface. On the other hand, the visible part of the spectrum produces fewer photoproducts.

Testing the effect of individual wavelengths for longer times of irradiation (up to 18 h), Fig. 5 confirmed the responsibility of the UV light for the generation of the aromatic compound(s). It also showed that the effect of different wavelengths has different weights due to the changes in intensity and wavelength. The shorter wavelength and/or higher intensity have a stronger effect on both the surface active and bulk species. The results highlight the significant impact of solar spectrum composition on reaction pathways. They also emphasize the importance of incorporating these variations into the photochemical models used in atmospheric science for more accurate predictions of the complex chemical interactions that occur in the atmosphere (Photochemical Air Quality Modeling; Xing et al., 2022).

16

17

18

19

20

21

22

23

24

25

26

27

28

29

30

31

32

33

34

7

8

9

10

11

12

13

14

15

4.2 Evolution of pH values

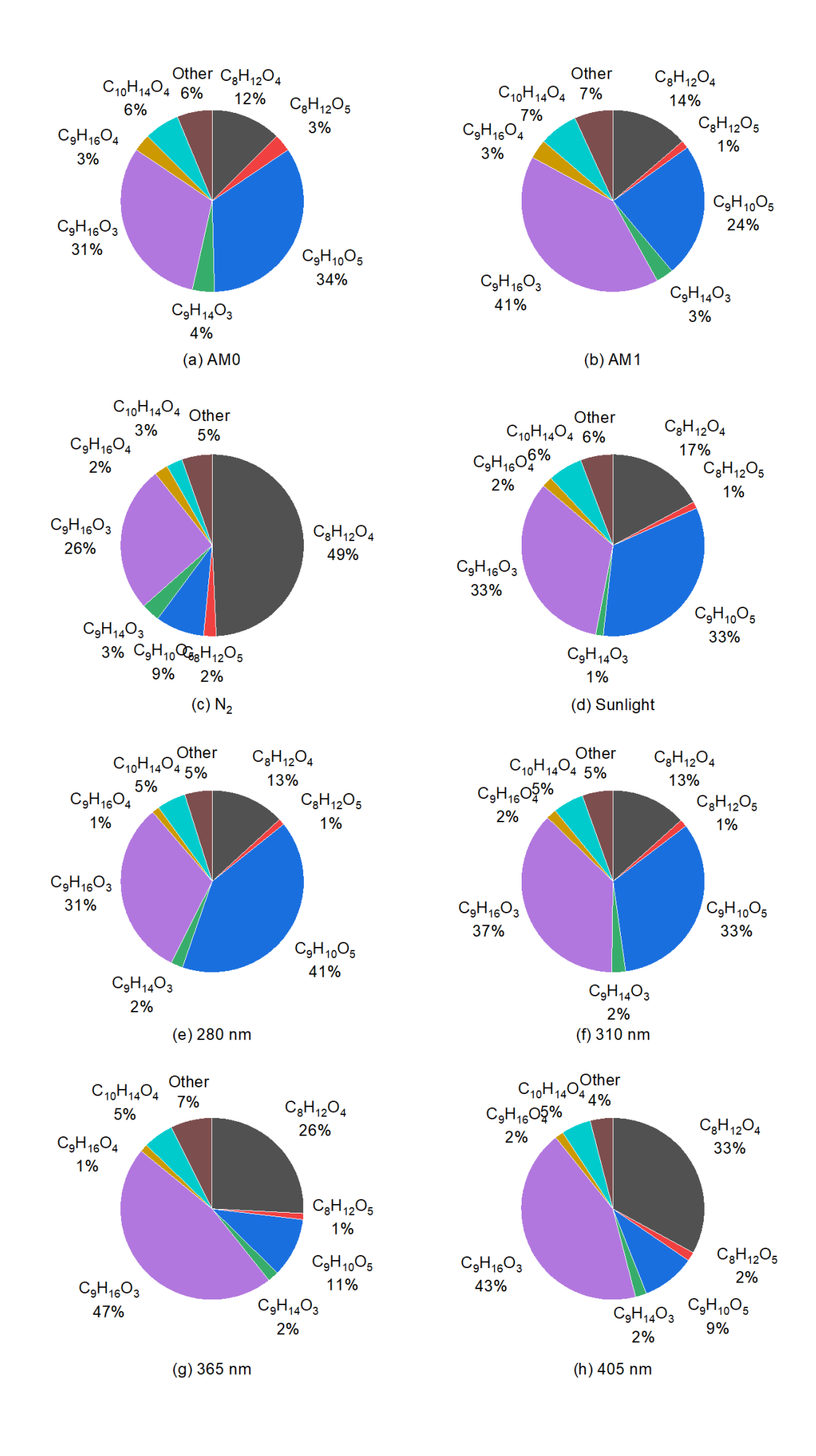
For solutions with a higher pH value of 8, a faster decrease in pH in the presence of 4-BBA after switching the UV light on (blue curve in Fig. S12). Under UV light irradiation, the 4-BBA molecule absorbs energy, leading to excitation. The excited state can undergo decarboxylation, where the carboxyl group (-COOH) is lost as carbon dioxide (CO₂), resulting in the formation of benzene and a carboxylic acid radical. The carbonation is the dissolution of carbon dioxide (CO₂) in water to form carbonic acid (H₂CO₃), which can further dissociate into bicarbonate (HCO₃⁻) and carbonate (CO₃²-) ions. The carbonation process is primarily influenced by the concentration of dissolved CO2 in water and the partial pressure of CO2 in the surrounding atmosphere. The pH of the solution can indirectly affect carbonation by influencing the equilibrium between carbonic acid and its dissociation products. The fast decrease in pH value under UV light for a solution with an initial ~pH 8 and containing 4-BBA is a laboratory issue due to the relatively high 4-BBA concentration in a limited sample volume. In nature, this effect is negligible, e.g. in large water reservoirs, but could become relevant, e.g. for cloud droplets. To understand the indirect effect of pH change on the SFG signal, we have to recall that the balance between the hydrophobic tail and the hydrophilic head controls the adsorption of surfactants. While hydrophobicity is directly connected with hydrocarbon length, hydrophilicity is mostly unquantified

(Rosen and Kunjappu, 2012). The hydrophilicity of head groups is qualitatively related to the

solvation and solubility. Thus, a nonionized state would be less hydrophilic than an ionized state because it would be less soluble. Normally, NA is only partially dissociated. The change in pH at a constant concentration of NA changes the concentration of NA at the surface and hence the surface pressure (Luo et al., 2020). Although the relationship between the surface pressure and the SFG signal at the air water interface is not well established, it is confirmed that the SFG signal may increase or decrease with surface pressure depending on a number of factors, such as the composition and arrangement of the molecules at the interface, the polarization of the incident light, and the concentration of adsorbed species (Feng et al., 2016). A side effect of pH change during the experiment is the change in the degree of protonation and deprotonation of 4-BBA at different pH values which affects its absorbance spectra (see Fig. S13) (Karimova et al., 2023). This increases the complexity of the photoreaction if the pH value is not constant during the irradiation process.

4.3 Reaction mechanism for the formation of major products

In all MS experiments, C₈H₁₂O₄, C₉H₁₀O₅, and C₉H₁₆O₃ were the most abundant products detected in the liquid phase. However, the fractions of the liquid phase compounds varied under different irradiation conditions, Fig. 13a to h. For C₉H₁₆O₃, which was formed through RO₂ radical reactions after hydrogen abstraction on NA (Tinel et al., 2016), the fraction in total liquid-phase C*H*,O* was higher with irradiation of AM1 than AM0 Fig. 13a and b. This stands in agreement with the measurement with irradiation from 280 nm to 405 nm, Fig. 13e to h. With more UV at 280 nm and 310 nm, C₉H₁₆O₃ accounted for about ~31 % and ~37 % of total C_xH_yO_z, respectively; while with less UV at 365 nm and 405 nm, the fractions of C₉H₁₆O₃ increased to ~47 % and ~43 %, respectively. In contrast, the fraction of C₉H₁₀O₅ in total liquid-phase C_xH_yO_z decreased from ~41 % at 280 nm to ~9 % at 405 nm. We also observed a higher fraction of ~34 % for C₉H₁₀O₅ at AMO, and a lower fraction of ~24 % at AM1. For C₉H₁₆O₃, the signals in the reference experiments in the absence of NA or 4-BBA were similar to that in the reference experiment in the absence of both NA and 4-BBA. However, we observed significant formation of C₉H₁₀O₅ in the experiment of 4-BBA alone, in which the intensity of C₂H₁₀O₅ was about half of that in the mixture of NA and 4-BBA experiment, suggesting that C₉H₁₀O₅ is very likely to be an aromatic compound formed through 4-BBA irradiation and the presence of NA could promote its formation. This conclusion is consistent with the presence of two different reaction mechanisms as inferred from Fig. 11. C₈H₁₂O₄ is a major product from the photoreaction of NA, and there is less dependence of the formation of C₈H₁₂O₄ on oxygen compared to other products. This leads to an increase of the fraction of C₈H₁₂O₄ in total liquid phase C_xH_yO_z in N₂ experiment, Fig. 13c.



1 Figure 13. Fractions of products in total liquid-phase C_xH_yO_z under different irradiation

2 conditions.

6

7

8

3 In previous work by Tinel et al. 2016, the solution with 4-BBA showed the formation of C₉H₁₆O₃

4 increased by a factor of ~2.5 in the presence of air. In our study, with 4-BBA the formation of C₉H₁₆O₃

5 increased by a factor of ~11. The oxygenated C₉ products are promoted when O₂ is abundant, which

is in agreement with Tinel et al. The promotion of oxygen on the formation of C₈H₁₂O₄ was limited.

The formation of C₈H₁₂O₄ was significantly improved with the presence of 4-BBA, indicating that

C₈H₁₂O₄ was a photodegradation product from NA. The following scheme shows the suggested

9 photolysis of 4-BBA alone:

10
$$4BBA(C_{14}H_{10}O_{3}) \xrightarrow{hv} C_{14}H_{11}O_{3}$$
11
$$C_{14}H_{11}O_{3} \xrightarrow{hv \leq 310 \text{ nm}, H_{2}O} C_{6}H_{6} + C_{8}H_{7}O_{3}$$
12
$$C_{14}H_{11}O_{3} \xrightarrow{hv \leq 310 \text{ nm}, H_{2}O} C_{7}H_{6}O + C_{7}H_{7}O_{2}$$
13
$$C_{9}H_{7}O_{2} \xrightarrow{O_{2},HCO_{3}} C_{9}H_{10}O_{5}$$

14 The photolysis of NA in the presence of 4-BBA could follow the following scheme:

15
$$4BBA(C_{14}H_{10}O_3) + C_9H_{18}O_2 \xrightarrow{hv} C_{14}H_{11}O_3 + C_9H_{12}O_2$$
16
$$C_9H_{17}O_2 \xrightarrow{O_2} C_9H_{17}O_4$$
17
$$C_9H_{17}O_4 \xrightarrow{RO_2} C_9H_{16}O_3 + C_9H_{18}O_3$$
18
$$C_9H_{17}O_4 \xrightarrow{O_2,HCO_3} C_{10}H_{14}O_4$$
19
$$C_9H_{16}O_2 \xrightarrow{hv,OH} C_9H_{16}O_2 + C_9H_{16}O_4$$

20 21

22

23

24

25

26

27

28

29

AM0 irradiation of NA solution without 4-BBA did not show any changes in the SFG signal indicating no photoreaction in the absence of 4-BBA, Fig. 1a. On the other hand, irradiating 4-BBA without NA with AM0 showed a slight decrease of the water bands at the very beginning followed by the recovery of the dark signal within one hour of irradiation, Fig. 1b. Although the changes in OH stretching modes from hydrogen-bonded interfacial water at ~3240 and 3450 cm⁻¹ are within the signal-to-noise, the change in the dangling OH band at ~3700 cm⁻¹ is noticeable. This is likely due to photodissociation of 4-BBA under UV light. Indeed, the results of the mass spectroscopy in the gas phase, blue bars in Fig. 12, confirm the dissociation of 4-BBA, after irradiation with AM0, and the emission of benzene and benzaldehyde in the absence of NA. A key question that arises is why the

aromatic band at 3070 cm⁻¹ is absent in the SFG spectrum (Fig. 1b) after irradiation, despite its 1 2 presence when irradiating the mixture in the presence of NA (Fig. 2b). The photolysis process can break chemical bonds within the molecule and rearrange the atoms, 3 resulting in the formation of new compounds. The specific conditions and reactions involved in the 4 5 photolysis of 4-benzoylbenzoic acid may vary depending on factors such as the intensity and 6 wavelength of the light, the presence of sensitizers or catalysts, and the reaction environment. The 7 photolysis of 4-BBA acid can involve multiple reaction pathways depending on the experimental 8 conditions and the nature of the light source. Benzene and benzaldehyde may form upon photolysis 9 of 4-BBA through two possible reaction pathways: 1) Decarboxylation, where the carboxyl group (-COOH) is lost as carbon dioxide (CO₂), resulting in the formation of benzene and a carboxylic acid 10 radical. The carboxylic acid radical can undergo further reactions, such as hydrogen abstraction or 11 rearrangements, potentially leading to the formation of benzaldehyde. 2) Photoreduction, where in 12 the presence of a suitable reducing agent (NA in our case), the photogenerated carboxylic acid radical 13 can undergo reduction reactions. If NA is present in the reaction mixture, it could potentially act as a 14 hydrogen donor or a radical scavenger. It could react with the photogenerated carboxylic acid radical, 15 accepting a hydrogen atom and undergoing oxidation itself in the process. This reaction could lead to 16 the formation of benzaldehyde as a primary product, along with other side products. Benzene can also 17 be formed through subsequent reactions, such as further reduction or rearrangement of the 18 intermediate products. The first pathway applies to the SFG experiment without NA, Fig. 1b, while 19 20 the second pathway additionally applies to the SFG experiments in the presence of NA and 4-BBA, 21 e.g. in Fig. 2b. 22 The appearance of the aromatic band in Fig. 2b but not in Fig. 1b after AM0 irradiation can be attributed to the properties of benzaldehyde. Benzaldehyde (C6H5CHO) is an aromatic aldehyde, 23 consisting of both a benzene ring and an aldehyde functional group (-CHO). While it has a polar 24 25 aldehyde group, the nonpolar nature of the benzene ring dominates, resulting in low solubility in water but a high affinity for organic compounds. Due to its predominantly nonpolar structure, 26 27 benzaldehyde lacks the hydrophilic-hydrophobic balance required to function as a surfactant. 28 Although its polar functional group may allow for weak interactions at the water surface, these 29 interactions are not strong enough to significantly reduce surface tension or exhibit notable surface activity. As a result, benzaldehyde does not appear in Fig. 1b. Surface activity or surfactant properties 30 are typically associated with amphiphilic molecules, which have both hydrophilic and hydrophobic 31 regions. These molecules can accumulate at interfaces and reduce the surface tension of the system. 32 33 This behavior arises from the orientation of surfactant molecules at the air-water interface, with their 34 hydrophilic portions interacting with water and their hydrophobic portions interacting with nonpolar

regions. On the other hand, in the presence of NA, and due to the high affinity, benzaldehyde appears 1 at the surface and could contribute to the SFG signal as can be seen in Fig. 2b. 2 Although, the aromatic band of benzaldehyde was not detected in the absence of NA, the impact of 3 its presence as a photoproduct appeared as a reduction in the dangling OH band after 30 min of AM0 4 irradiation, green curve Fig. 1b. The observed decrease in the dangling OH band intensity in the SFG 5 6 spectrum upon the emergence of benzaldehyde into water is indicative of the alteration of the 7 hydrogen bonding environment at the water surface due to the interaction between the benzaldehyde 8 photoproduct and water molecules. Benzaldehyde, being molecule with a polar carbonyl group (-9 CHO), can either interact directly with the dangling OH at the surface or form hydrogen bonds with water molecules through the oxygen atom of the aldehyde group. This interaction between 10 benzaldehyde and water can compete with the hydrogen bonding of water molecules to the dangling 11 OH groups at the water surface. As a result, the formation of benzaldehyde leads to a reduction in the 12 13 availability of free hydroxide ions causing a decrease in the intensity of the dangling OH peak 14 observed in the SFG spectrum after 30 min of irradiation. 15 One possible explanation for the increase after the decrease in the dangling OH band observed in the SFG spectrum after the formation of benzaldehyde is that initially, upon the formation of 16 benzaldehyde, its presence disrupts the hydrogen bonding network of water molecules at the water 17 surface as described above. There are two scenarios for the afterword increase of the dangling OH 18 signal. First, as the concentration of benzaldehyde increases beyond a certain threshold, a reverse 19 20 effect may occur, e.g. benzaldehyde molecules self-aggregate or form clusters at the water surface due to their nonpolar aromatic moiety. This clustering or aggregation can create local environments 21 that are more favorable for hydrogen bonding with water molecules leading to an increase in the 22 23 intensity of the dangling OH band in the SFG spectrum. The second scenario involves the evaporation 24 of benzaldehyde from the water surface due to its volatility. Benzaldehyde has a relatively low boiling 25 point of around 179-180 °C and a significant vapor pressure, which means it can readily transition from a liquid to a gas phase at room temperature. The second scenario is the more likely to occur as 26 27 is proven by the detection of benzaldehyde in the gas phase in the mass spectrometry results. 28 In the presence of NA, benzaldehyde and NA can interact due to their chemical properties. Benzaldehyde, with an aromatic ring and aldehyde group (CHO), and NA, with a carboxylic acid 29 30 group (-COOH), can engage in acid-base reactions. NA, a weak acid, can donate a proton, while benzaldehyde can accept it, potentially forming a conjugate acid. Additionally, they may undergo 31 32 other reactions like condensation, esterification, or oxidation, depending on the conditions and 33 presence of catalysts.

5-4 Conclusions

This study focuses on the correlation between the photochemical products at the surface and bulk 2 regions. We spotlighted the complex contribution of solar power-spectral distribution, pH, salinity 3 and surface photoproducts on the reaction mechanism. We chose nNAonanoic acid, was selected as 4 5 surfactant, and 4-BBA, as a photosensitizer, and our compared our combined surface-bulk study was compared to the bulk-phases study by Tinel et al., (2016) (Tinel et al., 2016). Our analysis revealed 6 7 several photoproducts in both the gas and liquid phases that were not reported in the reference study, while conversely, the reference study identified additional products not detected in our work. We 8 9 attribute these differences to differences in the analytical techniques used, differences in sample purity, and discrepancies in the spectral characteristics of the light sources applied. 10 The SFG technique allowed enabled us to detect and confirm the partition of the non-surface-active 11 compounds to the organic surface layer where it can induce radical reactions leading to the formation 12 of a variety of compounds. We also identified photoproducts at the water-air interface that cannot be 13 assigned by the bulk analysis. Under the environmental conditions applied in this work, the 4-BBA 14 was found to be acting as a source of photoproducts in addition to its expected role as a photosensitizer 15 for the NA. The photolysis of the 4-BBA is more active when exposed to shorter wavelengths of the 16 17 UV portion of the light spectrum. The subsequent reactions between the photoproducts can lead to 18 the formation of -aromatic compounds including compounds with amphipathic structures that are surface-active and responsible for the restructuring of the water molecules at the interface. Lower pH 19 20 values were found to be more favorable for the formation of these amphipathic aromatic compounds. Benzaldehyde, formed by the photolysis of 4-BBA, plays a vital role in the photosensitized chemistry 21 22 of NA at the surface. 23 The spectral power distribution of the day irradiation light significantly affects the photoreactions. 24 This indicates the importance of considering the geographical position, atmospheric conditions, and the time of day and year in the modeling parametrizations. The shorter wavelength and/or higher 25 intensity has stronger effect. The change in pH changes the concentration of partially dissociated fatty 26 acids at the surface and influences the photo reaction rate, and possibly pathways. Preliminary results 27 28 also showed that the salinity accelerates the photoreaction rate. We attributed this effect to the 29 increase in the concentration of the 4-BBA at the air-water interface caused by the bulk 30 dissolved salts. Further investigation of the mechanism under varying pH and salty conditions is necessary to be addressed in future work. Finally, dissolved oxygen develops multiple pathways of 31 the interactions. While our study provides valuable mechanistic insight, broader conclusions would 32 require further investigation using additional model systems and environmentally relevant mixtures. 33 In nature, these processes are even more complex due to the presence of a large variety of fatty acids 34

- 1 at the SML which enrich more organic photosensitizers at the surface. Similar These
- 2 findingsphotochemistry can apply to all water surfaces, e.g. at ocean, rivers, lakes and even cloud
- 3 droplets.

1 Author contribution

All authors have made significant contributions to this research. AA proposed the research idea, conducted the literature review, designed and built the custom solar simulator, and conceived and designed the experiments. AA led the SFG and MS experiments, performed data analysis and interpretation, and wrote and compiled the manuscript. DG conducted the SFG experiments alongside AA, contributed to the SFG data analysis, and provided critical revisions to the manuscript. DG additionally revised and corrected the chemical composition part of the MS study after Referee's reports. -YG performed the MS experiments, analyzed and interpreted the MS data in collaboration with AA and -drafted the MS-related sections, and revised the MS content of the manuscript. BB supervised the SFG experiments, discussed the results with AA and DG, and reviewed the SFG-related sections. HS supervised the MS experiments, discussed the results with AA and YG, and revised the MS sections. JL contributed to the chemistry aspects of the experiments, assisted with methodology development and data collection, and participated in manuscript revisions. MF supported the estimation and validation of the solar simulator output and characteristics and assisted in final manuscript preparation.

16

17

2

3

4

5

6

7

8

9

10

11

12

13

14

15

Acknowledgements

- AA gratefully acknowledges the support of the German Research Foundation (DFG, AB 604/3-1).
- 19 Special thanks are extended to Ottmar Möhler for hosting AA in his group at KIT during the
- 20 finalization of the manuscript following the conclusion of the DFG project. The authors thank Olga
- 21 Dombrowski for assistance with sample preparations in the chemistry lab at KIT and Thomas Leisner
- for hosting the first author at IMKAAF-KIT during the DFG project period. DG and BB thank the
- 23 DFG for funding CRC 1459 Intelligent Matter Project-ID 433682494. The authors acknowledge
- 24 the assistance of ChatGPT in refining the abstract, author contributions, and acknowledgments text
- 25 for improved clarity and professionalism.

26

27

Competing interests

- Some authors are members of the editorial board of journal ACP. The authors declare that there are
- 29 no conflicts of interest regarding the publication of this paper. No financial, personal, or professional
- relationships influenced the research or its outcomes.

31

32

33

Financial support

This research has been supported by the Deutsche Forschungsgemeinschaft (grant no. AB 604/3-1).

1 Supplementary information

- 2 Supplementary information related to this manuscript, including additional figures, tables, and
- 3 experimental procedures, is provided to support and enhance the understanding of the study. These
- 4 materials offer further insight into the methods and results discussed in the main text, ensuring a
- 5 comprehensive overview of the research.

78 Ethical approval

6

- 9 This article does not involve any studies or experiments conducted on human participants or animals
- by any of the authors.

1 References

- 2 Alpert, P. A., Ciuraru, R., Rossignol, S., Passananti, M., Tinel, L., Perrier, S., Dupart, Y., Steimer, S. S.,
- 3 Ammann, M., Donaldson, D. J., and George, C.: Fatty Acid Surfactant Photochemistry Results in New Particle
- 4 Formation, Sci. Rep., 7, https://doi.org/10.1038/s41598-017-12601-2, 2017.
- 5 Atkinson, R.: Atmospheric chemistry of VOCs and NOx, Atmos. Environ., 34, 2063–2101,
- 6 https://doi.org/10.1016/S1352-2310(99)00460-4, 2000.
- 7 Backus, E. H. G., Bonn, D., Cantin, S., Roke, S., and Bonn, M.: Laser-Heating-Induced Displacement of
- 8 Surfactants on the Water Surface, J. Phys. Chem. B, 116, 2703–2712, https://doi.org/10.1021/jp2074545,
- 9 2012.
- Badban, S., Hyde, A. E., and Phan, C. M.: Hydrophilicity of Nonanoic Acid and Its Conjugate Base at the
- 11 Air/Water Interface, ACS Omega, 2, 5565–5573, https://doi.org/10.1021/acsomega.7b00960, 2017.
- Bernard, F., Ciuraru, R., Boréave, A., and George, C.: Photosensitized Formation of Secondary Organic
- 13 Aerosols above the Air/Water Interface, Environ. Sci. Technol., 50, 8678-8686,
- 14 https://doi.org/10.1021/acs.est.6b03520, 2016.
- Boucher, O.: Atmospheric Aerosols, in: Atmospheric Aerosols: Properties and Climate Impacts, edited by:
- Boucher, O., Springer Netherlands, Dordrecht, 9–24, https://doi.org/10.1007/978-94-017-9649-1_2, 2015.
- Brüggemann, M., Hayeck, N., and George, C.: Interfacial photochemistry at the ocean surface is a global
- source of organic vapors and aerosols, Nat. Commun., 9, 2101, https://doi.org/10.1038/s41467-018-04528-7,
- 19 2018.
- 20 Carlson, D. J.: Dissolved organic materials in surface microlayers: Temporal and spatial variability and relation
- 21 to sea state, Limnol. Oceanogr., 28, 415–431, https://doi.org/10.4319/lo.1983.28.3.0415, 1983.
- 22 Carlson, D. J. and Mayer, L. M.: Enrichment of dissolved phenolic material in the surface microlayer of coastal
- 23 waters, Nature, 286, 482–483, https://doi.org/10.1038/286482a0, 1980.
- Carpenter, L. J. and Nightingale, P. D.: Chemistry and Release of Gases from the Surface Ocean, Chem. Rev.,
- 25 115, 4015–4034, https://doi.org/10.1021/cr5007123, 2015.
- 26 Ciuraru, R., Fine, L., van Pinxteren, M., D'Anna, B., Herrmann, H., and George, C.: Photosensitized
- production of functionalized and unsaturated organic compounds at the air-sea interface, Sci. Rep., 5, 12741,
- 28 https://doi.org/10.1038/srep12741, 2015.
- 29 Covington, A. K. and Whitfield, M.: Recommendations for the determination of pH in sea water and estuarine
- 30 waters, Pure Appl. Chem., 60, 865–870, https://doi.org/doi:10.1351/pac198860060865, 1988.
- 31 Cui, G., Liu, Y., and Tong, S.: Hydrogeochemical processes controlling the salinity of surface water and
- 32 groundwater in an inland saline-alkali wetland in western Jilin, China, Front. Ecol. Evol., 10,
- 33 https://doi.org/10.3389/fevo.2022.993849, 2022.
- Dalton, E. Z., Wang, X., Wappes, S. C., Petersen-Sonn, E. A., Hagan, S. N., George, C., and Raff, J. D.:
- 35 Photosensitizers Regulate Nitrate Photoproduct Yields in Bulk Aqueous Matrices, Environ. Sci. Technol., 59,
- 36 6142–6154, https://doi.org/10.1021/acs.est.4c09491, 2025.
- 37 Dickson, A. G.: The measurement of sea water pH, Mar. Chem., 44, 131–142, https://doi.org/10.1016/0304-
- 38 4203(93)90198-W, 1993.
- Dommer, A. C., Rogers, M. M., Carter-Fenk, K. A., Wauer, N. A., Rubio, P., Davasam, A., Allen, H. C., and
- 40 Amaro, R. E.: Interfacial Enrichment of Lauric Acid Assisted by Long-Chain Fatty Acids, Acidity and Salinity
- 41 at Sea Spray Aerosol Surfaces, J. Phys. Chem. A, 128, 7195–7207, https://doi.org/10.1021/acs.jpca.4c03335,
- 42 2024.
- Doughty, B., Yin, P. C., and Ma, Y. Z.: Adsorption, Ordering, and Local Environments of Surfactant-
- 44 Encapsulated Polyoxometalate Ions Probed at the Air-Water Interface, Langmuir, 32, 8116–8122,
- 45 https://doi.org/10.1021/acs.langmuir.6b01643, 2016.
- 46 Freeman-Gallant, G., Davis, E. J., Scholer, E., Alija, O., and Navea, J. G.: Photooxidation of Nonanoic Acid
- 47 by Molecular and Complex Environmental Photosensitizers, J. Phys. Chem. A, 128, 9792-9803,

- 1 https://doi.org/10.1021/acs.jpca.4c05608, 2024.
- 2 Gantt, B. and Meskhidze, N.: The physical and chemical characteristics of marine primary organic aerosol: a
- 3 review, Atmos. Chem. Phys., 13, 3979–3996, https://doi.org/10.5194/acp-13-3979-2013, 2013.
- 4 García Rey, N., Weißenborn, E., Schulze-Zachau, F., Gochev, G., and Braunschweig, B.: Quantifying Double-
- 5 Layer Potentials at Liquid-Gas Interfaces from Vibrational Sum-Frequency Generation, J. Phys. Chem. C,
- 6 123, 1279–1286, https://doi.org/10.1021/acs.jpcc.8b10097, 2019.
- 7 Gautam, K. S., Schwab, A. D., Dhinojwala, A., Zhang, D., Dougal, S. M., and Yeganeh, M. S.: Molecular
- 8 Structure of Polystyrene at Air/Polymer and Solid/Polymer Interfaces, Phys. Rev. Lett., 85, 3854–3857,
- 9 https://doi.org/10.1103/PhysRevLett.85.3854, 2000.
- 10 Ghosh, A., Campen, R. K., Sovago, M., and Bonn, M.: Structure and dynamics of interfacial water in model
- lung surfactants, Faraday Discuss., 141, 145–159, https://doi.org/10.1039/b805858j, 2009.
- Goswami, P. C., Mayo, P. de, Ramnath, N., Bernard, G., Omkaram, N., Scheffer, J. R., and Wong, Y.-F.:
- Modification of photochemical reactivity through the use of clathrates: the Norrish type I and type II reactions
- in Dianin's compound, Can. J. Chem., 63, 2719–2725, https://doi.org/10.1139/v85-451, 1985.
- 15 Gragson, D. E. and Richmond, G. L.: Investigations of the Structure and Hydrogen Bonding of Water
- Molecules at Liquid Surfaces by Vibrational Sum Frequency Spectroscopy, J. Phys. Chem. B, 102, 3847–
- 3861, https://doi.org/10.1021/jp9806011, 1998.
- Hardt, M., Honnigfort, C., Carrascosa-Tejedor, J., Braun, M. G., Winnall, S., Glikman, D., Gutfreund, P.,
- 19 Campbell, R. A., and Braunschweig, B.: Photoresponsive arylazopyrazole surfactant/PDADMAC mixtures:
- 20 reversible control of bulk and interfacial properties, Nanoscale, 16, 9975-9984,
- 21 https://doi.org/10.1039/D3NR05414D, 2024.
- Hendrickson, B. N., Brooks, S. D., Thornton, D. C. O., Moore, R. H., Crosbie, E., Ziemba, L. D., Carlson, C.
- A., Baetge, N., Mirrielees, J. A., and Alsante, A. N.: Role of Sea Surface Microlayer Properties in Cloud
- 24 Formation, Front. Mar. Sci., 7, https://doi.org/10.3389/fmars.2020.596225, 2021.
- 25 Henry, M. C., Yang, Y. J., Pizzolatto, R. L., and Messmer, M. C.: Competitive adsorption of 2,4,7,9-
- tetramethyl-5-decyn-4,7-diol and linear alkane surfactants at the air/water interface, Langmuir, 19, 2592–2598,
- 27 https://doi.org/10.1021/la026812l, 2003.
- Jiang, L. Q., Carter, B. R., Feely, R. A., Lauvset, S. K., and Olsen, A.: Surface ocean pH and buffer capacity:
- 29 past, present and future, Sci. Rep., 9, 18624, https://doi.org/10.1038/s41598-019-55039-4, 2019.
- 30 Jiménez, M. C. and Miranda, M. A.: Organic aspects. Oxygen-containing functions, 169–193,
- 31 https://doi.org/10.1039/9781788013598-00169, 2018.
- 32 Kroll, J. H., Lim, C. Y., Kessler, S. H., and Wilson, K. R.: Heterogeneous Oxidation of Atmospheric Organic
- 33 Aerosol: Kinetics of Changes to the Amount and Oxidation State of Particle-Phase Organic Carbon, J. Phys.
- 34 Chem. A, 119, 10767–10783, https://doi.org/10.1021/acs.jpca.5b06946, 2015.
- Kusaka, R., Ishiyama, T., Nihonyanagi, S., Morita, A., and Tahara, T.: Structure at the air/water interface in
- 36 the presence of phenol: a study using heterodyne-detected vibrational sum frequency generation and molecular
- 37 dynamics simulation, Phys. Chem. Chem. Phys., 20, 3002–3009, https://doi.org/10.1039/C7CP05150F, 2018.
- Lankone, R. S., Deline, A. R., Barclay, M., and Fairbrother, D. H.: UV–Vis quantification of hydroxyl radical
- 39 concentration and dose using principal component analysis, Talanta, 218, 121148,
- 40 https://doi.org/10.1016/j.talanta.2020.121148, 2020.
- Liss, P. S. and Duce, R. A.: The Sea Surface and Global Change, Cambridge University Press, 2005.
- 42 Lu, R., Gan, W., Wu, B., Zhang, Z., Guo, Y., and Wang, H.: C–H Stretching Vibrations of Methyl, Methylene
- and Methine Groups at the Vapor/Alcohol (n = 1-8) Interfaces, J. Phys. Chem. B, 109, 14118-14129,
- 44 https://doi.org/10.1021/jp051565q, 2005.
- 45 MacPhail, R. A., Strauss, H. L., Snyder, R. G., and Elliger, C. A.: Carbon-hydrogen stretching modes and the
- 46 structure of n-alkyl chains. 2. Long, all-trans chains, J. Phys. Chem., 88, 334–341.
- 47 https://doi.org/10.1021/j150647a002, 1984.
- 48 Marion, G. M., Millero, F. J., Camões, M. F., Spitzer, P., Feistel, R., and Chen, C. T. A.: pH of seawater, Mar.

- 1 Chem., 126, 89–96, https://doi.org/10.1016/j.marchem.2011.04.002, 2011.
- 2 Meerkötter, R. and Vázquez-Navarro, M.: Earth's Radiation Budget: The Driver for Weather and Climate, in:
- 3 Atmospheric Physics: Background Methods Trends, edited by: Schumann, U., Springer Berlin Heidelberg,
- 4 Berlin, Heidelberg, 55–67, https://doi.org/10.1007/978-3-642-30183-4_4, 2012.
- 5 Milinković, A., Penezić, A., Kušan, A. C., Gluščić, V., Žužul, S., Skejić, S., Šantić, D., Godec, R., Pehnec, G.,
- 6 Omanović, D., Engel, A., and Frka, S.: Variabilities of biochemical properties of the sea surface microlayer:
- 7 Insights to the atmospheric deposition impacts, Sci. Total Environ., 838, 156440,
- 8 https://doi.org/10.1016/j.scitotenv.2022.156440, 2022.
- 9 Millero, F. J., Feistel, R., Wright, D. G., and McDougall, T. J.: The composition of Standard Seawater and the
- definition of the Reference-Composition Salinity Scale, Deep Sea Res. Part I Oceanogr. Res. Pap., 55, 50–72,
- 11 https://doi.org/10.1016/j.dsr.2007.10.001, 2008.
- Miranda, P. B. and Shen, Y. R.: Liquid interfaces: A study by sum-frequency vibrational spectroscopy, J. Phys.
- 13 Chem. B, 103, 3292–3307, https://doi.org/10.1021/jp9843757, 1999.
- 14 Mmereki, B. T. and Donaldson, D. J.: Laser induced fluorescence of pyrene at an organic coated air-water
- interface, Phys. Chem. Chem. Phys., 4, 4186–4191, https://doi.org/10.1039/b204754c, 2002.
- Mora Garcia, S. L., Pandit, S., Navea, J. G., and Grassian, V. H.: Nitrous Acid (HONO) Formation from the
- 17 Irradiation of Aqueous Nitrate Solutions in the Presence of Marine Chromophoric Dissolved Organic Matter:
- 18 Comparison to Other Organic Photosensitizers, ACS Earth Sp. Chem., 5, 3056–3064,
- 19 https://doi.org/10.1021/acsearthspacechem.1c00292, 2021.
- 20 Morgan, J. J.: Aquatic Chemistry-Chemical Equilibria and Rates in Natural Waters, USA: JOHN WILEY,
- 21 1995.
- 22 Nihonyanagi, S., Mondal, J. A., Yamaguchi, S., and Tahara, T.: Structure and dynamics of interfacial water
- studied by heterodyne-detected vibrational sum-frequency generation, Annu Rev Phys Chem, 64, 579–603,
- 24 https://doi.org/10.1146/annurev-physchem-040412-110138, 2013.
- Numadate, N., Saito, S., Nojima, Y., Ishibashi, T., Enami, S., and Hama, T.: Direct Observation and
- 26 Quantitative Measurement of OH Radical Desorption During the Ultraviolet Photolysis of Liquid Nonanoic
- 27 Acid, J. Phys. Chem. Lett., 13, 8290–8297, https://doi.org/10.1021/acs.jpclett.2c02199, 2022.
- Ouafo-Leumbe, M. R., Galy-Lacaux, C., Liousse, C., Pont, V., Akpo, A., Doumbia, T., Gardrat, E., Zouiten,
- 29 C., Sigha-Nkamdjou, L., and Ekodeck, G. E.: Chemical composition and sources of atmospheric aerosols at
- 30 Djougou (Benin), Meteorol. Atmos. Phys., 130, 591–609, https://doi.org/10.1007/s00703-017-0538-5, 2018.
- van Pinxteren, M., Fomba, K. W., Triesch, N., Stolle, C., Wurl, O., Bahlmann, E., Gong, X., Voigtländer, J.,
- Wex, H., Robinson, T.-B., Barthel, S., Zeppenfeld, S., Hoffmann, E. H., Roveretto, M., Li, C., Grosselin, B.,
- Daële, V., Senf, F., van Pinxteren, D., Manzi, M., Zabalegui, N., Frka, S., Gašparović, B., Pereira, R., Li, T.,
- Wen, L., Li, J., Zhu, C., Chen, H., Chen, J., Fiedler, B., von Tümpling, W., Read, K. A., Punjabi, S., Lewis,
- A. C., Hopkins, J. R., Carpenter, L. J., Peeken, I., Rixen, T., Schulz-Bull, D., Monge, M. E., Mellouki, A.,
- George, C., Stratmann, F., and Herrmann, H.: Marine organic matter in the remote environment of the Cape
- George, C., Stratmann, F., and Herrmann, H.: Marine organic matter in the remote environment of the Cape
- Verde islands an introduction and overview to the MarParCloud campaign, Atmos. Chem. Phys., 20, 6921–
- 38 6951, https://doi.org/10.5194/acp-20-6921-2020, 2020.
- Rao, Y., Li, X., Lei, X. G., Jockusch, S., George, M. W., Turro, N. J., and Eisenthal, K. B.: Observations of
- 40 Interfacial Population and Organization of Surfactants with Sum Frequency Generation and Surface Tension,
- 41 J. Phys. Chem. C, 115, 12064–12067, https://doi.org/10.1021/jp201799z, 2011.
- 42 Riva, M., Rantala, P., Krechmer, J. E., Peräkylä, O., Zhang, Y., Heikkinen, L., Garmash, O., Yan, C., Kulmala,
- 43 M., Worsnop, D., and Ehn, M.: Evaluating the performance of five different chemical ionization techniques
- 44 for detecting gaseous oxygenated organic species, Atmos. Meas. Tech., 12, 2403-2421,
- 45 https://doi.org/10.5194/amt-12-2403-2019, 2019.
- 46 Schultz, M. J., Baldelli, S., Schnitzer, C., and Simonelli, D.: Aqueous Solution/Air Interfaces Probed with Sum
- Frequency Generation Spectroscopy, J. Phys. Chem. B, 106, 5313–5324, https://doi.org/10.1021/jp014466v,
- 48 2002.
- 49 Sellegri, K., O'Dowd, C. D., Yoon, Y. J., Jennings, S. G., and de Leeuw, G.: Surfactants and submicron sea
- 50 spray generation, J. Geophys. Res., 111, https://doi.org/10.1029/2005jd006658, 2006.

- 1 Sellegri, K., Simó, R., Wang, B., Alpert, P. A., Altieri, K., Burrows, S., Hopkins, F. E., Koren, I., McCoy, I.
- 2 L., Ovadnevaite, J., Salter, M., and Schmale, J.: Influence of open ocean biogeochemistry on aerosol and
- 3 clouds: Recent findings and perspectives, Elem Sci Anth, 12, https://doi.org/10.1525/elementa.2023.00058,
- 4 2024
- 5 Shen, Y. R.: Surface Properties Probed by Second-Harmonic and Sum-Frequency Generation, Nature, 337,
- 6 519–525, https://doi.org/10.1038/337519a0, 1989.
- 7 Shultz, M. J., Schnitzer, C., Simonelli, D., and Baldelli, S.: Sum frequency generation spectroscopy of the
- 8 aqueous interface: ionic and soluble molecular solutions, Int. Rev. Phys. Chem., 19, 123-153,
- 9 https://doi.org/10.1080/014423500229882, 2000.
- 10 Snyder, R. G., Strauss, H. L., and Elliger, C. A.: Carbon-hydrogen stretching modes and the structure of n-
- alkyl chains. 1. Long, disordered chains, J. Phys. Chem., 86, 5145–5150, https://doi.org/10.1021/j100223a018,
- 12 1982.
- 13 Sovago, M., Campen, R. K., Wurpel, G. W. H., Müller, M., Bakker, H. J., and Bonn, M.: Vibrational Response
- of Hydrogen-Bonded Interfacial Water is Dominated by Intramolecular Coupling, Phys. Rev. Lett., 100,
- 15 173901, https://doi.org/10.1103/PhysRevLett.100.173901, 2008.
- Stolle, C., Ribas-Ribas, M., Badewien, T. H., Barnes, J., Carpenter, L. J., Chance, R., Damgaard, L. R., Durán
- Quesada, A. M., Engel, A., Frka, S., Galgani, L., Gašparović, B., Gerriets, M., Hamizah Mustaffa, N. I.,
- Herrmann, H., Kallajoki, L., Pereira, R., Radach, F., Revsbech, N. P., Rickard, P., Saint, A., Salter, M.,
- 19 Striebel, M., Triesch, N., Uher, G., Upstill-Goddard, R. C., van Pinxteren, M., Zäncker, B., Zieger, P., and
- Wurl, O.: The MILAN Campaign: Studying Diel Light Effects on the Air–Sea Interface, Bull. Am. Meteorol.
- 21 Soc., 101, E146–E166, https://doi.org/10.1175/BAMS-D-17-0329.1, 2020.
- Tilstone, G. H., Airs, ruth L., Vicente, V. M., Widdicombe, C., and Llewellyn, C.: High concentrations of
- 23 mycosporine-like amino acids and colored dissolved organic matter in the sea surface microlayer off the
- 24 Iberian Peninsula, Limnol. Oceanogr., 55, 1835–1850, https://doi.org/10.4319/lo.2010.55.5.1835, 2010.
- Tinel, L., Rossignol, S., Bianco, A., Passananti, M., Perrier, S., Wang, X., Brigante, M., Donaldson, D. J., and
- George, C.: Mechanistic Insights on the Photosensitized Chemistry of a Fatty Acid at the Air/Water Interface,
- 27 Environ. Sci. Technol., 50, 11041–11048, https://doi.org/10.1021/acs.est.6b03165, 2016.
- Tinel, L., Abbatt, J., Saltzman, E., Engel, A., Fernandez, R., Li, Q., Mahajan, A. S., Nicewonger, M., Novak,
- 29 G., Saiz-Lopez, A., Schneider, S., and Wang, S.: Impacts of ocean biogeochemistry on atmospheric chemistry,
- 30 Elem Sci Anth, 11, https://doi.org/10.1525/elementa.2023.00032, 2023.
- 31 Truong, V. N. T., Wang, X. M., Dang, L. X., and Miller, J. D.: Interfacial Water Features at Air-Water
- 32 Interfaces as Influenced by Charged Surfactants, J. Phys. Chem. B, 123, 2397–2404,
- 33 https://doi.org/10.1021/acs.jpcb.9b01246, 2019.
- 34 Varga, I., Keszthelyi, T., Meszaros, R., Hakkel, O., and Gilanyi, T.: Observation of a liquid-gas phase
- transition in monolayers of alkyltrimethylammonium alkyl sulfates adsorbed at the air/water interface, J. Phys.
- 36 Chem. B, 109, 872–878, https://doi.org/10.1021/jp0480060, 2005.
- Wang, Y., Zeng, J., Wu, B., Song, W., Hu, W., Liu, J., Yang, Y., Yu, Z., Wang, X., and Gligorovski, S.:
- 38 Production of Volatile Organic Compounds by Ozone Oxidation Chemistry at the South China Sea Surface
- 39 Microlayer, ACS Earth Sp. Chem., 7, 1306–1313, https://doi.org/10.1021/acsearthspacechem.3c00102, 2023.
- Wilson, T. W., Ladino, L. A., Alpert, P. A., Breckels, M. N., Brooks, I. M., Browse, J., Burrows, S. M.,
- 41 Carslaw, K. S., Huffman, J. A., Judd, C., Kilthau, W. P., Mason, R. H., McFiggans, G., Miller, L. A., Najera,
- 42 J. J., Polishchuk, E., Rae, S., Schiller, C. L., Si, M., Temprado, J. V, Whale, T. F., Wong, J. P. S., Wurl, O.,
- 43 Yakobi-Hancock, J. D., Abbatt, J. P. D., Aller, J. Y., Bertram, A. K., Knopf, D. A., and Murray, B. J.: A marine
- 44 biogenic source of atmospheric ice-nucleating particles, Nature, 525, 234-+.
- 45 https://doi.org/10.1038/nature14986, 2015.
- 46 Xing, J., Zheng, S., Li, S., Huang, L., Wang, X., Kelly, J. T., Wang, S., Liu, C., Jang, C., Zhu, Y., Zhang, J.,
- 47 Bian, J., Liu, T.-Y., and Hao, J.: Mimicking atmospheric photochemical modeling with a deep neural network,
- 48 Atmos. Res., 265, 105919, https://doi.org/10.1016/j.atmosres.2021.105919, 2022.
- 49 Yan, S., Liu, Y., Lian, L., Li, R., Ma, J., Zhou, H., and Song, W.: Photochemical formation of carbonate radical
- 50 and its reaction with dissolved organic matters, Water Res., 161, 288–296,

- 1 https://doi.org/10.1016/j.watres.2019.06.002, 2019.
- 2 Yang, L., Zhang, J., Engel, A., and Yang, G.-P.: Spatio-temporal distribution, photoreactivity and
- 3 environmental control of dissolved organic matter in the sea-surface microlayer of the eastern marginal seas
- 4 of China, Biogeosciences, 19, 5251–5268, https://doi.org/10.5194/bg-19-5251-2022, 2022.
- 5 You, B., Li, S., Tsona, N. T., Li, J., Xu, L., Yang, Z., Cheng, S., Chen, Q., George, C., Ge, M., and Du, L.:
- 6 Environmental Processing of Short-Chain Fatty Alcohols Induced by Photosensitized Chemistry of Brown
- 7 Carbons, ACS Earth Sp. Chem., 4, 631–640, https://doi.org/10.1021/acsearthspacechem.0c00023, 2020.
- 8 Zhang, D., Gutow, J., and Eisenthal, K. B.: Vibrational-spectra, orientations, and phase-transitions in long-
- 9 chain amphiphiles at the air-water-interface probing the head and tail groups by sum-frequency generation,
- 10 J. Phys. Chem., 98, 13729–13734, https://doi.org/10.1021/j100102a045, 1994.
- 11 Alpert, P. A., Ciuraru, R., Rossignol, S., Passananti, M., Tinel, L., Perrier, S., Dupart, Y., Steimer, S. S.,
- 12 Ammann, M., Donaldson, D. J., and George, C.: Fatty Acid Surfactant Photochemistry Results in New Particle
- 13 Formation, Sci. Rep., 7, https://doi.org/10.1038/s41598-017-12601-2, 2017.
- 14 Backus, E. H. G., Bonn, D., Cantin, S., Roke, S., and Bonn, M.: Laser Heating Induced Displacement of
- Surfactants on the Water Surface, J. Phys. Chem. B, 116, 2703–2712, https://doi.org/10.1021/jp2074545,
- 16 2012.
- 17 Badban, S., Hyde, A. E., and Phan, C. M.: Hydrophilicity of Nonanoic Acid and Its Conjugate Base at the
- 18 Air/Water Interface, ACS Omega, 2, 5565–5573, https://doi.org/10.1021/acsomega.7b00960, 2017.
- 19 Bernard, F., Ciuraru, R., Boréave, A., and George, C.: Photosensitized Formation of Secondary Organic
- 20 Aerosols above the Air/Water Interface, Environ. Sci. Technol., 50, 8678 8686,
- 21 https://doi.org/10.1021/acs.est.6b03520, 2016.
- 22 Boucher, O.: Atmospheric Aerosols, in: Atmospheric Aerosols: Properties and Climate Impacts, edited by:
- 23 Boucher, O., Springer Netherlands, Dordrecht, 9 24, https://doi.org/10.1007/978-94-017-9649-1-2, 2015.
- 24 Brüggemann, M., Hayeck, N., and George, C.: Interfacial photochemistry at the ocean surface is a global
- source of organic vapors and aerosols, Nat. Commun., 9, 2101, https://doi.org/10.1038/s41467-018-04528-7,
- 26 2018.
- 27 Carlson, D. J.: Dissolved organic materials in surface microlayers: Temporal and spatial variability and relation
- 28 to sea state, Limnol. Oceanogr., 28, 415-431, https://doi.org/10.4319/lo.1983.28.3.0415, 1983.
- 29 Carlson, D. J. and Mayer, L. M.: Enrichment of dissolved phenolic material in the surface microlayer of coastal
- 30 waters, Nature, 286, 482-483, https://doi.org/10.1038/286482a0, 1980.
- 31 Carpenter, L. J. and Nightingale, P. D.: Chemistry and Release of Gases from the Surface Ocean, Chem. Rev.,
- 32 115, 4015 4034, https://doi.org/10.1021/cr5007123, 2015.
- 33 Ciuraru, R., Fine, L., van Pinxteren, M., D'Anna, B., Herrmann, H., and George, C.: Photosensitized
- 34 production of functionalized and unsaturated organic compounds at the air-sea interface, Sci. Rep., 5, 12741,
- 35 https://doi.org/10.1038/srep12741, 2015.
- 36 Covington, A. K. and Whitfield, M.: Recommendations for the determination of pH in sea water and estuarine
- 37 waters, Pure Appl. Chem., 60, 865–870, https://doi.org/doi:10.1351/pac198860060865, 1988.
- 38 Dickson, A. G.: The measurement of sea water pH, Mar. Chem., 44, 131–142, https://doi.org/10.1016/0304-
- 39 4203(93)90198 W, 1993.
- 40 Dommer, A. C., Rogers, M. M., Carter Fenk, K. A., Wauer, N. A., Rubio, P., Davasam, A., Allen, H. C., and
- 41 Amaro, R. E.: Interfacial Enrichment of Lauric Acid Assisted by Long Chain Fatty Acids, Acidity and Salinity
- 42 at Sea Spray Aerosol Surfaces, J. Phys. Chem. A, 128, 7195-7207, https://doi.org/10.1021/acs.jpca.4c03335,
- 43 2024.
- 44 Doughty, B., Yin, P. C., and Ma, Y. Z.: Adsorption, Ordering, and Local Environments of Surfactant-
- 45 Encapsulated Polyoxometalate Ions Probed at the Air Water Interface, Langmuir, 32, 8116 8122,
- 46 https://doi.org/10.1021/acs.langmuir.6b01643, 2016.
- 47 Photochemical Air Quality Modeling: https://www.epa.gov/scram/photochemical-air quality-modeling.
- 48 Gantt, B. and Meskhidze, N.: The physical and chemical characteristics of marine primary organic aerosol: a

- 1 review, Atmos. Chem. Phys., 13, 3979-3996, https://doi.org/10.5194/acp-13-3979-2013, 2013.
- 2 García Rey, N., Weißenborn, E., Schulze Zachau, F., Gochev, G., and Braunschweig, B.: Quantifying Double-
- 3 Layer Potentials at Liquid Gas Interfaces from Vibrational Sum Frequency Generation, J. Phys. Chem. C,
- 4 123, 1279 1286, https://doi.org/10.1021/acs.jpcc.8b10097, 2019.
- 5 Gautam, K. S., Schwab, A. D., Dhinojwala, A., Zhang, D., Dougal, S. M., and Yeganeh, M. S.: Molecular
- 6 Structure of Polystyrene at Air/Polymer and Solid/Polymer Interfaces, Phys. Rev. Lett., 85, 3854-3857,
- 7 https://doi.org/10.1103/PhysRevLett.85.3854, 2000.
- 8 Ghosh, A., Campen, R. K., Sovago, M., and Bonn, M.: Structure and dynamics of interfacial water in model
- 9 lung surfactants, Faraday Discuss., 141, 145–159, https://doi.org/10.1039/b805858j, 2009.
- 10 Hardt, M., Honnigfort, C., Carrascosa Tejedor, J., Braun, M. G., Winnall, S., Glikman, D., Gutfreund, P.,
- 11 Campbell, R. A., and Braunschweig, B.: Photoresponsive arylazopyrazole surfactant/PDADMAC mixtures:
- 12 reversible control of bulk and interfacial properties, Nanoscale, 16, 9975 9984,
- 13 https://doi.org/10.1039/D3NR05414D, 2024.
- 14 Hendrickson, B. N., Brooks, S. D., Thornton, D. C. O., Moore, R. H., Crosbie, E., Ziemba, L. D., Carlson, C.
- 15 A., Baetge, N., Mirrielees, J. A., and Alsante, A. N.: Role of Sea Surface Microlayer Properties in Cloud
- 16 Formation, Front. Mar. Sci., 7, https://doi.org/10.3389/fmars.2020.596225, 2021.
- 17 Henry, M. C., Yang, Y. J., Pizzolatto, R. L., and Messmer, M. C.: Competitive adsorption of 2,4,7,9
- 18 tetramethyl 5 decyn 4,7 diol and linear alkane surfactants at the air/water interface, Langmuir, 19, 2592 2598,
- 19 https://doi.org/10.1021/la0268121, 2003.
- 20 Jiang, L. Q., Carter, B. R., Feely, R. A., Lauvset, S. K., and Olsen, A.: Surface ocean pH and buffer capacity:
- 21 past, present and future, Sci. Rep., 9, 18624, https://doi.org/10.1038/s41598-019-55039-4, 2019.
- 22 Liss, P. S. and Duce, R. A.: The Sea Surface and Global Change, Cambridge University Press, 2005.
- 23 Lu, R., Gan, W., Wu, B., Zhang, Z., Guo, Y., and Wang, H.: C-H Stretching Vibrations of Methyl, Methylene
- 24 and Methine Groups at the Vapor/Alcohol (n = 1-8) Interfaces, J. Phys. Chem. B, 109, 14118-14129,
- 25 https://doi.org/10.1021/jp051565q, 2005.
- 26 MacPhail, R. A., Strauss, H. L., Snyder, R. G., and Elliger, C. A.: Carbon-hydrogen stretching modes and the
- 27 structure of n-alkyl chains. 2. Long, all trans chains, J. Phys. Chem., 88, 334-341,
- 28 https://doi.org/10.1021/j150647a002, 1984.
- 29 Marion, G. M., Millero, F. J., Camões, M. F., Spitzer, P., Feistel, R., and Chen, C. T. A.: pH of seawater, Mar.
- 30 Chem., 126, 89–96, https://doi.org/10.1016/j.marchem.2011.04.002, 2011.
- 31 Meerkötter, R. and Vázquez Navarro, M.: Earth's Radiation Budget: The Driver for Weather and Climate, in:
- 32 Atmospheric Physics: Background Methods Trends, edited by: Schumann, U., Springer Berlin Heidelberg,
- 33 Berlin, Heidelberg, 55 67, https://doi.org/10.1007/978-3-642-30183-4_4, 2012.
- 34 Milinković, A., Penezić, A., Kušan, A. C., Gluščić, V., Žužul, S., Skejić, S., Šantić, D., Godec, R., Pehnec, G.,
- 35 Omanović, D., Engel, A., and Frka, S.: Variabilities of biochemical properties of the sea surface microlayer:
- 36 Insights to the atmospheric deposition impacts, Sci. Total Environ., 838, 156440,
- 37 https://doi.org/10.1016/j.scitotenv.2022.156440, 2022.
- 38 Millero, F. J., Feistel, R., Wright, D. G., and McDougall, T. J.: The composition of Standard Seawater and the
- definition of the Reference Composition Salinity Scale, Deep Sea Res. Part I Oceanogr. Res. Pap., 55, 50-72,
- 40 https://doi.org/10.1016/j.dsr.2007.10.001, 2008.
- 41 Miranda, P. B. and Shen, Y. R.: Liquid interfaces: A study by sum-frequency vibrational spectroscopy, J. Phys.
- 42 Chem. B, 103, 3292–3307, https://doi.org/10.1021/jp9843757, 1999.
- 43 Mmereki, B. T. and Donaldson, D. J.: Laser induced fluorescence of pyrene at an organic coated air water
- 44 interface, Phys. Chem. Chem. Phys., 4, 4186–4191, https://doi.org/10.1039/b204754c, 2002.
- 45 Mora Garcia, S. L., Pandit, S., Navea, J. G., and Grassian, V. H.: Nitrous Acid (HONO) Formation from the
- 46 Irradiation of Aqueous Nitrate Solutions in the Presence of Marine Chromophoric Dissolved Organic Matter:
- 47 Comparison to Other Organic Photosensitizers, ACS Earth Sp. Chem., 5, 3056 3064,
- 48 https://doi.org/10.1021/acsearthspacechem.1c00292, 2021.

- 1 Morgan, J. J.: Aquatic Chemistry Chemical Equilibria and Rates in Natural Waters, USA: JOHN WILEY,
- 2 1995.
- 3 Nihonyanagi, S., Mondal, J. A., Yamaguchi, S., and Tahara, T.: Structure and dynamics of interfacial water
- 4 studied by heterodyne detected vibrational sum frequency generation, Annu Rev Phys Chem, 64, 579–603,
- 5 https://doi.org/10.1146/annurev-physchem-040412-110138, 2013.
- 6 Ouafo-Leumbe, M. R., Galy-Lacaux, C., Liousse, C., Pont, V., Akpo, A., Doumbia, T., Gardrat, E., Zouiten,
- 7 C., Sigha Nkamdjou, L., and Ekodeck, G. E.: Chemical composition and sources of atmospheric aerosols at
- 8 Djougou (Benin), Meteorol. Atmos. Phys., 130, 591–609, https://doi.org/10.1007/s00703-017-0538-5, 2018.
- 9 van Pinxteren, M., Fomba, K. W., Triesch, N., Stolle, C., Wurl, O., Bahlmann, E., Gong, X., Voigtländer, J.,
- 10 Wex, H., Robinson, T. B., Barthel, S., Zeppenfeld, S., Hoffmann, E. H., Roveretto, M., Li, C., Grosselin, B.,
- 11 Daële, V., Senf, F., van Pinxteren, D., Manzi, M., Zabalegui, N., Frka, S., Gašparović, B., Pereira, R., Li, T.,
- Wen, L., Li, J., Zhu, C., Chen, H., Chen, J., Fiedler, B., von Tümpling, W., Read, K. A., Punjabi, S., Lewis,
- 13 A. C., Hopkins, J. R., Carpenter, L. J., Peeken, I., Rixen, T., Schulz-Bull, D., Monge, M. E., Mellouki, A.,
- 14 George, C., Stratmann, F., and Herrmann, H.: Marine organic matter in the remote environment of the Cape
- 15 Verde islands—an introduction and overview to the MarParCloud campaign, Atmos. Chem. Phys., 20, 6921—
- 16 6951, https://doi.org/10.5194/acp-20-6921-2020, 2020.
- 17 Rao, Y., Li, X., Lei, X. G., Jockusch, S., George, M. W., Turro, N. J., and Eisenthal, K. B.: Observations of
- 18 Interfacial Population and Organization of Surfactants with Sum Frequency Generation and Surface Tension,
- 19 J. Phys. Chem. C, 115, 12064–12067, https://doi.org/10.1021/jp201799z, 2011.
- 20 Schultz, M. J., Baldelli, S., Schnitzer, C., and Simonelli, D.: Aqueous Solution/Air Interfaces Probed with Sum
- 21 Frequency Generation Spectroscopy, J. Phys. Chem. B, 106, 5313-5324, https://doi.org/10.1021/jp014466v,
- 22 2002.
- 23 Sellegri, K., O'Dowd, C. D., Yoon, Y. J., Jennings, S. G., and de Leeuw, G.: Surfactants and submicron sea
- 24 spray generation, J. Geophys. Res., 111, https://doi.org/10.1029/2005jd006658, 2006.
- 25 Shen, Y. R.: Surface Properties Probed by Second-Harmonic and Sum-Frequency Generation, Nature, 337,
- 26 519 525, https://doi.org/10.1038/337519a0, 1989.
- 27 Shultz, M. J., Schnitzer, C., Simonelli, D., and Baldelli, S.: Sum frequency generation spectroscopy of the
- 28 aqueous interface: ionic and soluble molecular solutions, Int. Rev. Phys. Chem., 19, 123 153,
- 29 https://doi.org/10.1080/014423500229882, 2000.
- 30 Snyder, R. G., Strauss, H. L., and Elliger, C. A.: Carbon hydrogen stretching modes and the structure of n-
- 31 alkyl chains. 1. Long, disordered chains, J. Phys. Chem., 86, 5145-5150, https://doi.org/10.1021/j100223a018,
- 32 1982.
- 33 Sovago, M., Campen, R. K., Wurpel, G. W. H., Müller, M., Bakker, H. J., and Bonn, M.: Vibrational Response
- 34 of Hydrogen Bonded Interfacial Water is Dominated by Intramolecular Coupling, Phys. Rev. Lett., 100,
- 35 173901, https://doi.org/10.1103/PhysRevLett.100.173901, 2008.
- 36 Stolle, C., Ribas-Ribas, M., Badewien, T. H., Barnes, J., Carpenter, L. J., Chance, R., Damgaard, L. R., Durán
- 37 Quesada, A. M., Engel, A., Frka, S., Galgani, L., Gašparović, B., Gerriets, M., Hamizah Mustaffa, N. I.,
- 38 Herrmann, H., Kallajoki, L., Pereira, R., Radach, F., Revsbech, N. P., Rickard, P., Saint, A., Salter, M.,
- 39 Striebel, M., Triesch, N., Uher, G., Upstill Goddard, R. C., van Pinxteren, M., Zäncker, B., Zieger, P., and
- Surface, iv., These, i., one, o., openin-bound, k. c., van i materia, vi., zaneker, b., zieger, i., and
- 40 Wurl, O.: The MILAN Campaign: Studying Diel Light Effects on the Air Sea Interface, Bull. Am. Meteorol.
- 41 Soc., 101, E146-E166, https://doi.org/10.1175/BAMS-D-17-0329.1, 2020.
- 42 Tilstone, G. H., Airs, ruth L., Vicente, V. M., Widdicombe, C., and Llewellyn, C.: High concentrations of
- 43 mycosporine like amino acids and colored dissolved organic matter in the sea surface microlayer off the
- 44 Iberian Peninsula, Limnol. Oceanogr., 55, 1835–1850, https://doi.org/10.4319/lo.2010.55.5.1835, 2010.
- 45 Tinel, L., Rossignol, S., Bianco, A., Passananti, M., Perrier, S., Wang, X., Brigante, M., Donaldson, D. J., and
- 46 George, C.: Mechanistic Insights on the Photosensitized Chemistry of a Fatty Acid at the Air/Water Interface,
- 47 Environ. Sci. Technol., 50, 11041 11048, https://doi.org/10.1021/acs.est.6b03165, 2016.
- 48 Truong, V. N. T., Wang, X. M., Dang, L. X., and Miller, J. D.: Interfacial Water Features at Air-Water
- 49 Interfaces as Influenced by Charged Surfactants, J. Phys. Chem. B, 123, 2397 2404,
- 50 https://doi.org/10.1021/acs.jpcb.9b01246, 2019.

- 1 Varga, I., Keszthelyi, T., Meszaros, R., Hakkel, O., and Gilanyi, T.: Observation of a liquid gas phase
- 2 transition in monolayers of alkyltrimethylammonium alkyl sulfates adsorbed at the air/water interface, J. Phys.
- 3 Chem. B, 109, 872–878, https://doi.org/10.1021/jp0480060, 2005.
- 4 Wang, Y., Zeng, J., Wu, B., Song, W., Hu, W., Liu, J., Yang, Y., Yu, Z., Wang, X., and Gligorovski, S.:
- 5 Production of Volatile Organic Compounds by Ozone Oxidation Chemistry at the South China Sea Surface
- 6 Microlayer, ACS Earth Sp. Chem., 7, 1306–1313, https://doi.org/10.1021/acsearthspacechem.3c00102, 2023.
- Wilson, T. W., Ladino, L. A., Alpert, P. A., Breckels, M. N., Brooks, I. M., Browse, J., Burrows, S. M.,
- 8 Carslaw, K. S., Huffman, J. A., Judd, C., Kilthau, W. P., Mason, R. H., McFiggans, G., Miller, L. A., Najera,
- 9 J. J., Polishchuk, E., Rae, S., Schiller, C. L., Si, M., Temprado, J. V. Whale, T. F., Wong, J. P. S., Wurl, O.,
- 10 Yakobi Hancock, J. D., Abbatt, J. P. D., Aller, J. Y., Bertram, A. K., Knopf, D. A., and Murray, B. J.: A marine
- 11 biogenic source of atmospheric ice nucleating particles, Nature, 525, 234+,
- 12 https://doi.org/10.1038/nature14986, 2015.

22

- 13 Xing, J., Zheng, S., Li, S., Huang, L., Wang, X., Kelly, J. T., Wang, S., Liu, C., Jang, C., Zhu, Y., Zhang, J.,
- 14 Bian, J., Liu, T.-Y., and Hao, J.: Mimicking atmospheric photochemical modeling with a deep neural network,
- 15 Atmos. Res., 265, 105919, https://doi.org/10.1016/j.atmosres.2021.105919, 2022.
- 16 Yang, L., Zhang, J., Engel, A., and Yang, G. P.: Spatio temporal distribution, photoreactivity and
- 17 environmental control of dissolved organic matter in the sea surface microlayer of the eastern marginal seas
- 18 of China, Biogeosciences, 19, 5251 5268, https://doi.org/10.5194/bg-19-5251-2022, 2022.
- 19 Zhang, D., Gutow, J., and Eisenthal, K. B.: Vibrational spectra, orientations, and phase transitions in long-
- 20 chain amphiphiles at the air-water interface probing the head and tail groups by sum frequency generation,
- 21 J. Phys. Chem., 98, 13729 13734, https://doi.org/10.1021/j100102a045, 1994.